Towards a tracer-based conceptualization of meltwater dynamics and streamflow response in a glacierized catchment

Running title: Meltwater dynamics and streamflow response

Daniele Penna[1], Michael Engel[2], Giacomo Bertoldi[3], Francesco Comiti[2]

[1]Department of Agricultural, Food and Forestry Systems, University of Florence, via San Bonaventura 13, 50145 Florence-Firenze, Italy.
[2]Faculty of Science and Technology, Free University of Bozen-Bolzano, Piazza dell' Università 5, 39100, Bozen-Bolzano, Italy.
[3]Institute for Alpine Environment, European Academy-EURAC, viale Druso 1, 39100, Bozen-Bolzano, Italy

Correspondence to: Daniele Penna (daniele.penna@unifi.it)

Abstract

Multiple water sources and the physiographic heterogeneity of glacierized catchments hamper a complete conceptualization of runoff response to meltwater dynamics. In this study, we used environmental tracers (stable isotopes of water and electrical conductivity) to obtain new insight into the hydrology of glacierized catchments, using the Saldur River catchment, Italian Alps, as a pilot site. We analysed the controls on the spatial and temporal patterns of the tracer signature in the main stream, its selected tributaries, shallow groundwater, snowmelt and glacier melt over a three-year period. We found that stream water electrical conductivity and isotopic composition showed consistent patterns in snowmelt-dominated periods whereas the streamflow contribution of glacier melt altered the correlations between the two tracers. By applying two- and three-component mixing models we quantified the seasonally-variable proportion of groundwater, snowmelt and glacier melt at different locations along the stream. We provided four model scenarios based on different tracer signatures of the end-members: the highest contributions of snowmelt to streamflow occurred in late spring-early summer and ranged between 70 % and 79 %, according to different scenarios, whereas the largest inputs by glacier melt were observed in mid-summer, and ranged between 57 % and 69 %. In addition to the identification of the main sources of uncertainty, we demonstrated how a careful sampling design is critical in order to avoid underestimation of the meltwater component in streamflow. The results of this study supported the development of a conceptual model of streamflow response to meltwater dynamics in the Saldur catchment likely valid for other glacierized catchments worldwide.

Keywords: snowmelt; glacier melt; groundwater; stable isotopes of water; electrical conductivity; glacierized catchment.

1. Introduction

Glacierized catchments are highly dynamic systems characterized by large complexity and heterogeneity due to the interplay of several geomorphic, ecological, climatic and hydrological processes. Particularly, the hydrology of glacierized catchments significantly impacts downstream settlements, ecosystems and larger catchments that are directly dependent on water deriving from snowmelt, glacier melt or high-elevation springs (Finger et al., 2013; Engelhardt et al., 2014). Water seasonally melting from snowpack and glacier bodies can constitute a larger contribution to annual streamflow than rain (Cable et al., 2011; Jost et al., 2012), and is widely used, especially in Alpine valleys, for irrigation and hydropower production (Schaefli et al., 2007; Beniston, 2012). It is therefore pivotal for an effective adoption of water resources strategies to understand the origin of water and to quantify the proportion of snowmelt and glacier melt in streamflow (Finger et al., 2013; Fan et al., 2015). To achieve this goal it is critical to gain a more detailed understanding of the hydrological functioning of glacierized catchments through the analysis of the spatial and temporal variability of water sources and the spatial and seasonal meltwater (snowmelt plus glacier melt) dynamics.

Hydrochemical tracers (e.g., stable isotopes of water, major ions, electrical conductivity (EC)) are among the most commonly employed tools to characterize hydrological dynamics in glacierized catchments (see Baraer et al. (2015) and references therein). In high-elevation catchments, the temporary storage of winter-early spring precipitation in the snowpack and in the glacier body and their melting during the late spring and summer controls the variability in solute and isotopic compositions of stream water (Kendall and McDonnell, 1998). Therefore, hydrochemical tracers allow for an effective identification of water sources and their variability within the catchments and over different seasons, providing essential information about water partitioning and water dynamics and improving our understanding of complex hydrology and hydroclimatology of the catchment (Rock and Mayer, 2007; Fan et al., 2015; Xing et al., 2015). Particularly, a few works relied on stable isotopes of water (^{2}H and ^{18}O) used in combination with EC to evaluate the role played by meltwater in the hydrology of glacierized catchments. For instance, some of these investigations allowed for the separation of streamflow into subglacial, englacial, melt and rainfall-derived components in the South Cascade Glacier, USA (Vaughn and Fountain, 2005), into components due to monsoon rainfall runoff, post-monsoon interflow, winter snowmelt and groundwater (the latter estimated up to 40 % during summer and monsoon periods) in the Ganga River, Himalaya (Maurya et al., 2011), and into snowmelt, ice melt and shallow groundwater components in Arctic catchments characterized by a gradient of glacierization (Blaen et al., 2014). Other researchers assessed the possibility to use isotopes and EC as complementary tracers, in addition to water temperature, to identify a permafrost-related component in spring water in a glacierized catchment in the Ortles-Cevedale massif, Italian Alps (Carturan et al., in press).

Two recent studies used stable isotopes and EC over a three-year period to assess water origin and streamflow contributors in the glacierized Saldur River catchment, Italian Alps. Penna et al. (2014) showed a preliminary analysis on the highly complex EC and isotopic signature of different waters sampled in the catchment, identifying distinct tracer signals in snowmelt and glacier melt. These two end-members dominated the streamflow throughout the late spring and summer, whereas liquid precipitation played a secondary role, limited to rare intense rainfall events. They also assessed, without quantifying it, the switch from snowmelt- to glacier melt-dominated periods, and estimated that the snowmelt fraction in groundwater ranged between 21 % and 93 %. Engel et al. (2016) employed two- and three-component mixing models to quantify the relative contribution of snowmelt, glacier melt and groundwater to streamflow during seven representative melt-induced runoff events sampled at high frequency at two cross-sections of the Saldur River. They observed marked reactions of tracers and streamflow both to melt and rainfall inputs, identifying

hysteretic loops of contrasting directions. They estimated the maximum contribution of snowmelt during June and July events (up to 33 %) and of glacier melt during the August events (up to 65 %). However, a quantification of the variations of streamflow components not only at the seasonal scale but also at different spatial scales across the catchment was not performed and a conceptual model of meltwater dynamics not presented. Therefore, despite the number of studies that have conducted hydrological tracer-based investigations in high-elevation mountain catchments, there is still the need to gain a better comprehension of the factors determining the complex hydrochemical signature of stream water and groundwater in glacierized catchments.

This research builds on the existing database for the Saldur River and on the first results presented in Penna et al. (2014) and Engel et al. (2016) to improve the knowledge on the complex hydrology and the water source dynamics in glacierized catchments. Specifically, we aim to:

- assess the controls on the spatial and temporal variability of the isotopic composition and EC in the main stream, tributaries and springs in the Saldur River catchment;
- quantify the proportion of snowmelt and glacier melt in streamflow at different stream locations and at different times of the year, as well as the related uncertainty;
- analyse the relation between the tracer signature and streamflow variability;
- derive a conceptual model of streamflow response to meltwater dynamics.

2. Study area

The research has been conducted in the upper portion of the Saldur/Saldura River catchment, Vinschgau/Venosta Valley, Eastern Italian Alps (Fig. 1). The catchment size is 61.7 km^2 and altitude ranges between 1632 m a.s.l. at the outlet (46°42'42.37"N, 10°38'51.41"E) and 3725 m a.s.l.. A glacier lies in the upper part of the catchment, with an extension of 2.28 km^2 in 2013, i.e., approximately 4% of total catchment area (Galos and Kaser, 2014). The glacier lost 21 % of its area from 2005 to 2013 (Galos, 2013). Several glacier-fed and non-glacier-fed lateral tributaries contribute to the Saldur River streamflow, and various springs, apparently connected or not connected to the main stream, can be found on the valley floor and at the toe of the hillslopes in the mid-upper part of the catchment. Rocks are metamorphic, mainly gneisses, mica-gneisses and schists. Land cover changes with elevation typically varying from Alpine forests (up to about 2200 m a.s.l.) to shrubs to Alpine grassland, bare soil and rocks above 2700 m a.s.l.. The area is characterized by a continental climate with average annual air temperature of 6.6 °C and precipitation as low as 569 mm/yr (at 1570 m a.s.l.), likely increasing up to 800-1000 mm/yr in the upper parts of the catchment. At 3000 m a.s.l., the total precipitation can be estimated, using the approach of Mair et al. (2015), to be about 1500 mm, 80% of which falls as snow. The hydrological regime is typically nivo-glacial with minimum streamflow recorded in winter and high flows occurring from late spring to mid-summer, when marked diurnal streamflow cycles occur, related to snow- and glacier melt (Mutzner et al., 2015). More detailed information on the study area are reported in Mao et al. (2014) and Penna et al. (2014).

3. Materials and methods

3.1 Hydrological and meteorological measurements

Field measurements were conducted from April 2011 to October 2013. Meteorological data were recorded at 15-min temporal resolution by two stations located at 2332 m a.s.l. and 1998 m a.s.l. (Fig. 1a). Stage in the Saldur River was recorded every 10 minutes by pressure transducers at the catchment outlet and at two river sections labelled Lower

120 Stream Gauge (S3-LSG, 2150 m a.s.l.) and Upper Stream Gauge (S5-USG, 2340 m a.s.l.), that defined two nested

121 subcatchments with an area of 18.6 km^2 and 11.2 km^2, respectively (Fig. 1a). Streamflow values were obtained by 82

122 discharge measurements acquired by the salt dilution method during various hydrometric conditions over the three

123 study years. Water level was also continuously measured on a left tributary (T2-SG, 2027 m a.s.l., Fig. 1b) draining an

124 area of 1.7 km^2 but a robust rating curve was not available to derive streamflow.

125

126 **3.2 Tracer sampling and measurement**

127 Samples analysed for the two tracers were collected from snowmelt, glacier melt, stream water and groundwater.

128 Snowmelt was sampled in late spring-early summer from water dripping from the residual snowpack at different

129 elevations and different locations. Snowmelt was sampled on three occasions in summer 2012 (end of June, beginning

130 and end of July), at elevations roughly between 2150 m a.s.l. and 2350 m a.s.l., and on nine occasions in summer 2013

131 (June, July and August) at elevations roughly between 2150 m a.s.l. and 2600 m a.s.l.. Glacier melt was sampled from

132 small rivulets flowing on the glacier surface, roughly at 2800 m a.s.l. in July and August 2012, and in July, August and

133 September 2013. Grab stream water samples were taken approximately monthly at eight locations in the Saldur River

134 (labelled from S1 to S8), at elevations spanning from 1809 m a.s.l. (S1) and 2415 m a.s.l. (S8), and from five tributaries

135 (labelled from T1 to T5), at elevations between 1775 m a.s.l. (T1) and 2415 m a.s.l. (T5, Fig. 1b). Samples at T1 were

136 taken only in 2012, and samples at T3 only in 2011. In 2013 samples were collected monthly during clear days only

137 from the river at four sections (S1, S3-LSG, S5-LSG, S8), respecting the same time of the day on each occasion in order

138 to ensure consistency and comparability between measurements. The representativeness of these samples for the typical

139 melting conditions in the catchment was visually ensured by comparing the hydrographs of the sampled days with the

140 ones of the corresponding months during the three monitored years. No wells are available in the study catchment, thus

141 spring water was assumed to represent shallow groundwater (Kong and Pang, 2012; Racoviteanu et al., 2013). Four

142 springs (labelled from SPR1 to SPR4) localized near the outlet of USG, between 2334 m a.s.l. and 2360 m a.s.l. were

143 sampled monthly during the three study years. On one occasion (17 October 2011), no sample was taken from SPR1

144 because it was found dry. Additionally, monthly samples were also taken from June to September 2013 from two

145 springs on the left valley hillslope, SPR6 and SPR7, at 2512 m a.s.l. and 2336 m a.s.l., respectively (Fig. 1b). A list of

146 all sampling locations with their main characteristics is reported in Penna et al. (2014).

147 In addition to the monthly sampling, stream water samples were collected at USG and LSG during seven runoff events

148 induced by meltwater in July and August 2011, and June, July and August 2012 and 2013. Samples were collected from

149 10:00 of one day to 10:00 (or longer) on the following day at hourly frequency during the day, until 22:00, and every

150 three hours during the night. For those events, two- and three-component mixing models were applied to quantify the

151 fraction of snowmelt and glacier melt in streamflow. Description of the runoff events and hydrograph separation results

152 are reported in Engel et al. (2016). The number of samples collected from the different water sources at the various

153 locations and years used in this study is reported in Table 1.

154

155 EC was determined directly in the field by means of a conductivity meter with a precision of $\pm$ 0.1 μS/cm. The EC

156 meter was routinely calibrated to ensure consistency among the measurements. Grab water samples for isotopic

157 determination were taken by 50 mL HDPE bottles with two caps and completely filled to avoid head space. Isotopic

158 analysis was carried out by an off-axis integrated cavity output spectroscope tested for precision, accuracy and memory

159 effect in previous intercomparison studies (Penna et al., 2010; 2012). The observed instrumental precision, considered

as the long-term average standard deviation, is 0.5 ‰ for δ^2H and 0.08 ‰ for δ^{18}O. Isotopic values are presented using the δ notation referred to the SMOW2-SLAP2 scale provided by the International Atomic Energy Agency.

3.3 Two- and three-component mixing models and underlying assumptions

A one-tracer, two-component mixing model (Pinder and Jones, 1969; Sklash and Farvolden, 1979) was used to quantify and separate two streamflow components (groundwater and snowmelt), and a two-tracer, three-component mixing model (Ogunkoya and Jenkins, 1993) was used for three streamflow components (groundwater, snowmelt and glacier melt). Mixing models were applied only to 2013 data because in that year water samples were collected at four locations along the main stream (S1, S3-LSG, S5-USG and S8) at the same time of the day on all sampling occasions. This was critical to ensure comparability of the results, given the high diurnal variability of streamflow and associated isotopic composition and EC, especially during the summer. In addition, results from the application of the two- and three-component mixing models to data collected hourly during seven melt-induced runoff events presented in Engel et al. (2016) were also used in this study for comparison purposes (see Section 4.3).

The following simplifying assumptions were made for the application of the mixing models:
- Streamflow at each selected sampling location of the Saldur River was a mixture of two components, viz. groundwater and snowmelt, or three components, viz. groundwater, snowmelt and glacier melt. The influence of precipitation was considered negligible because samples were collected during non-rainy periods, and particularly during warm, clear days when the meltwater input to runoff was remarkable and overwhelmed the possible presence of rain water in streamflow.
- The largest contribution of snowmelt to streamflow was assumed to derive from snow melting at an approximate elevation of 2800 m a.s.l.. The elevation band between 2800 m a.s.l. and 2850 m a.s.l. was the one with the largest area in the catchment (3.4 km^2), where much snow can accumulate, as confirmed by the analysis of snow cover data from Moderate-resolution Imaging Spectroradiometer (MODIS) images (c.f. Engel et al., 2016).

The three-component mixing model was based on isotopic and EC data (Maurya et al., 2011; Penna et al., 2015) and first applied to all samples collected in the Saldur River in 2013. When the three-component mixing model yielded inconsistent results, typically in May and June and partially in October, it was inferred that there was no glacier melt component in streamflow, thus the two-component mixing model was performed to separate the snowmelt from the groundwater component. As a preliminary step, both EC and isotopes were used in the two-component mixing model. The resulting estimates were strongly correlated ($p < 0.01$) but, overall, snowmelt fractions computed for May and June using isotopes were smaller compared to those computed through EC. In agreement with our previous work in the Saldur catchment (Engel et al., 2016), we decided to present EC-based results for the sampling days in May and June because of the large difference between the low EC of the snowmelt end-member and the relatively high EC of the stream that provided lower uncertainties in the estimated fractions compared to isotopes (Genereux et al., 1998). Conversely, for the sampling day in October, there was a relatively small difference between the EC of the groundwater end-member and the EC of the stream, while the difference in the isotopic signal of the end-members was greater, and thus the uncertainty in the estimated fractions was lower. Therefore, in these cases we used isotopes instead of EC in the two-component mixing model.

Based on the stated assumptions, the following mass balance equations can be written for periods when only snowmelt and groundwater contributed to streamflow:

$$SF = SM + GW \qquad \text{(Eq. 1)}$$

$$1 = sm + gw \qquad \text{(Eq. 2)}$$

$$\delta_{SF} = sm \cdot \delta_{SM} + gw \cdot \delta_{GW} \qquad \text{(Eq. 3)}$$

and

$$EC_{SF} = sm \cdot EC_{SM} + gw \cdot EC_{GW} \qquad \text{(Eq. 4)}$$

where SM, GW, and SF denote snowmelt, groundwater and streamflow, respectively; sm and gw indicate the streamflow fraction due to snowmelt and groundwater, respectively; and the notations δ and EC are used for the isotopic composition and the EC of each component, respectively. Eqs. 1-4 can be solved for the unknown sm as follows:

$$sm(\%) = \frac{\delta_{SF} - \delta_{GW}}{\delta_{SM} - \delta_{GW}} \cdot 100 \qquad \text{(Eq. 5)}$$

or, using EC:

$$sm(\%) = \frac{EC_{SF} - EC_{GW}}{EC_{SM} - EC_{GW}} \cdot 100 \qquad \text{(Eq. 6)}$$

The gw component can then be calculated by Eq. 2. Analogously, the following mass balance equations can be written for periods when snowmelt, glacier melt and groundwater contributed to streamflow:

$$SF = SM + GM + GW \qquad \text{(Eq. 7)}$$

$$1 = sm + gm + gw \qquad \text{(Eq. 8)}$$

$$\delta_{SF} = sm \cdot \delta_{SM} + gm \cdot \delta_{GM} + gw \cdot \delta_{GW} \qquad \text{(Eq. 9)}$$

$$EC_{SF} = sm \cdot EC_{SM} + gm \cdot EC_{GM} + gw \cdot EC_{GW} \qquad \text{(Eq. 10)}$$

where, in additions to the symbols used in Eqs. 1-6, GM denotes glacier melt, and gm indicates the streamflow fraction due to glacier melt. Eqs. 7-10 can be solved for the unknown sm and gm as follows:

$$sm\,(\%) = \frac{(\delta_{SF} - \delta_{GW}) \cdot (EC_{GM} - EC_{GW}) - (\delta_{GM} - \delta_{GW}) \cdot (EC_{SF} - EC_{GW})}{(\delta_{SM} - \delta_{GW}) \cdot (EC_{GM} - EC_{GW}) - (\delta_{GM} - \delta_{GW}) \cdot (EC_{SM} - EC_{GW})} \cdot 100 \qquad \text{(Eq. 11)}$$

$$gm\,(\%) = \frac{(\delta_{SF} - \delta_{GW}) \cdot (EC_{SM} - EC_{GW}) - (\delta_{SM} - \delta_{GW}) \cdot (EC_{SF} - EC_{GW})}{(\delta_{GM} - \delta_{GW}) \cdot (EC_{SM} - EC_{GW}) - (\delta_{SM} - \delta_{GW}) \cdot (EC_{GM} - EC_{GW})} \cdot 100 \qquad \text{(Eq. 12)}$$

The gw component can be then calculated by Eq. 8.

The uncertainty of the end-member fractions calculated through the two-component mixing model was quantified following the method of Genereux (1998) at the 70 % confidence level. The uncertainty of the end-member fractions calculated through the three-component mixing model was determined by varying the isotopic composition and EC of each end-member by $\pm$ 1 standard deviation (Carey and Quinton, 2005; Engel et al., 2016). All mixing models were applied using both δ^2H and δ^{18}O data; however, results based on δ^{18}O measurements showed a greater uncertainty than those derived from δ^2H data due to the instrumental performance (Penna et al., 2010). Thus, all results related to isotopes reported in this study are based on δ^2H data.

3.4. Scenarios of mixing model application

The spatial and temporal variability of end-member tracer signal is usually very difficult to characterize at the catchment-scale (Hoeg et al., 2000), especially in glacierized catchments (Jeelani et al., 2016), and it can noticeably affect the uncertainty of the results of mixing models. Since field measurements cannot reliably capture such a large spatial and temporal variability, we identified four different scenarios of mixing model application assuming that they

239   were representative for this variability. The four scenarios differed considering the groundwater end-member based on

240   springs or stream locations during baseflow conditions, and time-invariant or monthly-variable isotopic composition

241   and EC of the snowmelt end-member (Table 2). Particularly, in scenarios A and C, the groundwater end-member was

242   based on the average isotopic composition and EC of samples taken from springs during baseflow conditions in fall of

243   the three study years (springs were not sampled during winter due to limited accessibility of the area), consistently with

244   Engel et al. (2016) (Table 3) and assuming a negligible influence of the inter-annual variability of the climatic forcing

245   on the tracer signal of spring water during baseflow. In scenarios B and D, the groundwater end-member was defined as

246   the average of the tracer signal of different stream samples taken during baseflow conditions (late fall and winter of the

247   three study years), at the four Saldur River locations selected in 2013 (Table 3). For the definition of these two

248   groundwater end-members, we selected the samples taken during baseflow conditions when we assumed that there was

249   no or negligible contribution of snowmelt, glacier melt and rainfall to streamflow. It is important to note that we

250   consider as groundwater component both the spring baseflow and the stream baseflow, because the hydrochemistry of

251   streams during baseflow conditions generally integrates and reflects the hydrochemistry of the (shallow) groundwater at

252   the catchment scale (Sklash, 1990; Klaus and McDonnell, 2013; Fischer et al., 2015).

253

254   In scenarios A and B the tracer signature of the snowmelt end-member was considered time-invariant (Maurya et al.,

255   2011) (Table 4). Following Engel et al. (2016), the high-elevation (2800 m a.s.l.,) snowmelt isotopic composition was

256   identified through the regression analysis of snowmelt samples collected at different elevations in June 2013, according

257   to Eq. 13 ($R^2 = 0.616$, n = 7, $p < 0.05$):

258    $\delta^2 H\ (‰) = -0.0705 \cdot \text{elevation (m a.s.l.)} + 37.261$ (Eq. 13)

259   EC_{SM} was based on the average EC of all snowmelt samples collected in 2013, without applying any regression-based

260   modification.

261   In scenarios C and D, the isotopic composition of high-elevation snowmelt end-member was considered seasonally-

262   variable, to take into account that water from the melting snowpack typically undergoes progressive fractionation and

263   isotopic enrichment over the season (Taylor et al., 2001; Lee et al., 2010) (c.f. Section 4.1). A depletion rate of -7.0 ‰ in

264    $\delta^2 H$ for 100 m of elevation rise was derived from Eq. 13, and used to estimate the isotopic composition of high-elevation

265   snowmelt from snowmelt samples collected monthly at different elevations from May to August 2013 (Table 4).

266   Analogously, the average EC of snowmelt samples taken monthly was adopted.

267   In scenarios A and B, Eq. 13 was applied to snowmelt samples collected at different elevations (lower than 2800 m a.s.l.)

268   in order to estimate the average isotopic composition of high-elevation snowmelt, and thus to define a temporally-fixed

269   end-member isotopic composition that was used in the calculations of streamflow component fractions for each sampling

270   date (Table 4, scenarios A and B). In scenarios C and D, Eq. 13 was applied to snowmelt samples collected at different

271   elevations (lower than 2800 m a.s.l.) and at different times of the melting season in order to estimate the seasonally-

272   variable isotopic compositions of high-elevation snowmelt, that were used in the calculations of streamflow component

273   fractions for each sampling (Table 4, scenarios C and D).

274   For all scenarios, the isotopic signature and EC of the glacier melt end-member was considered monthly-variable (Table

275   5 and Section 4.1).

276

277   **4. Results**

278   **4.1 Isotopic composition and EC of the different water sources**

279 Snowmelt sampled from snow patches in summer 2012 and 2013 ranged in δ^2H from -106.1 ‰ to -139.5 ‰ and in EC

280 from 3.2 µS/cm and 77.0 µS/cm. Glacier melt displayed a marked enrichment in heavy isotopes over summer,

281 particularly in 2013 (Table 5). The spatial variability in the isotopic composition of glacier melt was generally small,

282 with spatial standard deviations ranging between 1.3 ‰ and 6.5 ‰. The EC of glacier melt was very low and little

283 variable in space and in time (average: 2.1 µS/cm, standard deviation: 0.7 µS/cm, n = 16) for 2012 and 2013 overall,

284 even though a slight progressive increase in EC was observed in 2013 (Table 5).

286 The Saldur catchment was characterized by a marked variability of tracer signature within the same water compartment

287 (i.e., main stream water, tributary water, groundwater) both in time and in space (Table 6, Fig. 2 and 3). There was a

288 statistically significant difference in δ^2H and EC between the Saldur River and its sampled tributaries for the entire

289 sampling period (Mann-Whitney test with p=0.004 and p<0.001, respectively). On average, stream water showed more

290 isotopically negative and variable values and had lower EC and higher variability in summer than in fall and winter.

291 Moreover, the main stream had more depleted isotopic composition and lower EC compared to the tributaries (Table 6).

292 Spring water was the most enriched water source during the fall but became more depleted compared to stream water

293 during the summer when it also showed higher EC. The coefficient of variations of δ^2H for groundwater were generally

294 slightly higher than for the stream water in all seasons, but the variability in EC was similar to that of the Saldur River

295 and smaller than that of the tributaries (Table 6).

297 Overall, the median isotopic composition of stream water in the Saldur River varied slightly with locations, but long

298 error bars indicate a great temporal variability (Fig. 2). On the contrary, tributaries showed a wider range in the isotopic

299 composition but a smaller temporal variability compared to the main stream (Fig. 2a). EC showed an increasing trend

300 from upper to lower locations along the Saldur River (although with a slight interruption at S3-LSG) (Fig. 2b).

301 Interestingly, T4 was the stream location with the most negative isotopic composition and highest EC. Groundwater

302 tracer signature was overall intermediate between the main stream and the tributaries with a remarkable difference

303 between SPR1-3 and SPR4.

304 Despite the strong variability, some spatial and temporal patterns can be observed (Fig. 3). For instance, all locations in

305 June and early July 2012 showed isotopically depleted water and so did, overall, locations T4 and T5. Groundwater in

306 SPR4 was constantly more enriched than in the other springs (Fig. 3a). The increasing trend in EC from the highest

307 Saldur River location (S8) down to the lowest location (S1) in July and August of both years is also clearly visible, as

308 well as the temporally constant and relatively very high EC of tributary water at T4 and very low EC of groundwater in

309 SPR4 (Fig. 3b).

311 The mixing-plot between δ^2H and EC of stream water and groundwater of all sampling locations further highlights the

312 differences in the tracer signature of the main stream, the tributaries and the springs (Fig. 4). Overall, the main stream

313 showed a wider range in isotopic composition compared to the tributaries, in agreement with the long error bars of

314 locations S1-S8 in Fig. 2. EC of the Saldur River was also more variable than EC in the other waters, except for T5 that

315 plots separately compared to other tributaries and the main stream. The spring data points only partially overlap with the

316 main stream data points: indeed, the tracer signal of the main stream water is upper-bounded by springs SPR1-3 and

317 partially by T2-SG, and laterally, towards the less negative isotopic values, by SPR4. Only the tracer signal of T1, a left

318 tributary flowing into the Saldur River a few hundred meters downstream S1, lies within the main stream data, but

319 samples were taken only in 2012 and so a robust comparison cannot be performed.

4.2 Quantification of snowmelt and glacier melt in streamflow and associated uncertainty

The results of the two- and three-component mixing models applied to 2013 data reveal a seasonally-variable influence of snowmelt and glacier melt on streamflow, with estimated fractions generally decreasing from the highest to the lowest sampling location (Fig. 5). Overall, the proportion of snowmelt in stream water was comparable for the four sampling locations in August, September and October. Estimated snowmelt fractions were highest on 19 June, up to 79 $\pm$ 6 % (scenario B) at S8. Field observations and MODIS data (Engel et al., 2016) revealed that the glacier surface was still covered with snow until the end of June. All four mixing model scenarios agree with these observations and estimate no contribution of glacier melt to streamflow on the sampling days in May and June, and only partially on 18 October (Fig. 5). Glacier melt was an important component of streamflow on 16 July, especially according to scenarios A and B, and dominated the streamflow in mid-August according to all scenarios, with peak estimates at S8 ranging from 50 - 66 % (scenario D) to 68 - 71 % (scenario A). On 12 August, meltwater was the prevalent streamflow component at the three upper sampling locations and was still relevant at the lowest sampling location.

Overall, the four scenarios provide similar patterns of meltwater dynamics with higher similarities between scenarios A and B, and between scenarios C and D. Indeed, strong correlations exist between the estimates of the same component computed in each scenario, with R^2 for all possible combinations ranging between 0.91 and 0.997 for groundwater, 0.68 and 0.94 for snowmelt, and 0.74 and 0.94 for glacier melt (n = 22, p < 0.01 for all correlations). Despite the general agreement, differences in the estimated streamflow components among the four scenarios do exist. Particularly, scenarios C and D yield higher overall proportions of snowmelt compared to scenarios A and B, and scenarios A and D provide the overall highest and smallest fraction of glacier melt, respectively. Furthermore, scenarios C and D provide larger proportions of snowmelt and smaller proportions of glacier melt in July compared to the two other scenarios (Fig. 5). Overall, the uncertainty associated with the computation of the streamflow fractions is larger for scenarios A and C than for scenarios B and D (compare the length of error bars in Fig. 5).

It is worth mentioning that different proportions of meltwater components at the same stream location could be estimated according to the sampling time of the day. For the melt-induced runoff events sampled at high temporal resolution in 2011, 2012 and 2013 (Engel et al., 2016), the maximum contribution of meltwater to streamflow occurred at the streamflow peak or within an hour after the streamflow peak in 79 % of the observations, whereas the maximum contribution of meltwater was observed within two hours before the streamflow peak in the remaining 21 % of the cases. Therefore, sampling several hours before or after the streamflow peak can lead to an underestimation of the meltwater fractions in streamflow (Fig. 6). However, the differences in meltwater fractions between samples collected at the streamflow peak and samples collected after the streamflow peak are lower and less variable (shorter error bars) than the ones computed before the streamflow peak (Fig. 6).

4.3 Relation between the two tracers, streamflow and meltwater fractions

The relation between δ^2H and EC of stream water samples collected at S5-USG and S3-LSG on the same days in 2011, 2012 and 2013, and grouped by month, shows different behaviours according to the sampling period (Fig. 7). Overall, sampling days in May, June and September were characterized by lower mean daily temperatures and stream discharge, much higher EC and more depleted isotopic composition compared to sampling days in July and August (Table 7). The relation between the two tracers is statistically significant in the colder months whereas it is more scattered and not statistically significant during the warmest months (Fig. 7). The range of δ^2H values was slightly larger in the mid-

361   summer period compared to May, June and September (16.7 ‰ vs. 15.1 ‰); on the contrary, the range of EC values

362   was much larger in the spring-late summer period compared to July and August (173.9 µS/cm vs. 77.1 µS/cm).

363

364   Streamflow during the summer melt runoff events sampled hourly in 2011, 2012 and 2013 at the two monitored cross

365   sections S5-USG and S3-LSG (Engel et al., 2016) is positively correlated with the fraction of meltwater (snowmelt plus

366   glacier melt components) (Fig. 8). Streamflow is presented for comparison purposes both in terms of specific discharge

367   and relative to bankfull discharge, the latter estimated in the two reaches based on direct observations during high

368   flows. A closer inspection of the figure reveals the occurrence of hysteretic loops between streamflow and meltwater at

369   both locations more evident for events on 12-13 July 2011, 10-11 August 2011 and 21-22 August 2013 at S5-USG, due

370   to their magnitude. Nevertheless, a general positive trend between the two variables is observable, with meltwater

371   fractions increasing when streamflow increased ($R^2 = 0.48$, n = 130; p < 0.01 at S5-USG; $R^2 = 0.26$, n = 114; p < 0.01 at

372   S3-LSG). The relation between meltwater fractions (computed as average of the results of the four mixing model

373   scenarios) and streamflow is also plotted for the samples taken monthly in 2013, indicated by the stars in Fig. 8. The

374   samples collected during the 2013 campaigns plot consistently with the samples taken during the melt-induced runoff

375   events at both locations, overall agreeing with the positive trend of the meltwater-streamflow relation (Fig. 8).

376

377   **5. Discussion**

378   **5.1 Controls on the spatio-temporal patterns of the tracer signal**

379   Glacier melt was characterized by similar isotopic composition in 2012 and 2013 and, most of all, by a marked isotopic

380   enrichment and a slight EC increase over the summer season (Table 5). Yde et al. (2016) showed similar trends in the

381   isotopic composition of meltwater draining Mittivakkat Gletscher, Greenland, for two summers, and Zhou et al. (2014)

382   reported an isotopic enrichment in the firnpack during the early melting season on a glacier in the Tibetan Plateau.

383   However, other studies have reported a strong inter-annual variability in the isotopic signature of glacier melt

384   (Yuanqing et al., 2001) or fairly consistent values over time (Cable et al., 2011; Maurya et al., 2011; Ohlanders et al.,

385   2013; Racoviteanu et al., 2013). In our case, since melting of the surface ice determines no isotopic fractionation

386   (Jouzel and Souchez,1982), as confirmed by glacier melt samples falling on the local meteorological water line (Penna

387   et al., 2014), the progressive enrichment could be explained by contributions from deeper portions of the glacier surface

388   with increasing ablation over the melting season or sublimation of surface ice (Stichler et al., 2001). More data from

389   this and other glacierized sites should be acquired to better assess this variability that we believe must be taken into

390   account in the application of mixing models for the estimation of glacier melt contribution to streamflow in different

391   seasons.

392

393   More negative δ^2H values and lower EC observed in the Saldur River and in its tributaries during the summer than

394   during the winter (Table 6) clearly indicate contributions of meltwater, namely snowmelt, typically isotopically

395   depleted, and glacier melt, typically very diluted in solutes. However, differences exist in the tracer signal among the

396   main stream and the tributaries. The much lower EC of the Saldur River in summer compared to the tributaries (Table

397   6) suggest important contributions of both snowmelt from high-elevations and almost solute-free glacier melt to the

398   main stream, but less glacier melt contributions to the tributaries. The larger difference of the coefficients of variation

399   between summer and fall-winter in the Saldur River with respect to the tributaries (Table 6) confirms greater inputs of

400   waters with contrasting isotopic signals (depleted snowmelt and more enriched glacier melt) but relatively similar low

401   EC (Maurya et al., 2011). This observation is corroborated by the larger temporal variability (longer error bars) in the

402 isotopic composition of the main stream compared to the tributaries, by the similar temporal variability in EC

403 (expressed by the similar length of error bars in Fig. 2), and by the larger span of δ^2H values in the main stream

404 compared to the tributaries visible in the mixing plot (Fig. 4).

405

406 The same isotopic composition of the Saldur River and the springs (Table 6, despite the lack of temporal consistency)

407 and the partial overlap of the spring data points with the stream data points in the mixing plot (Fig. 4) suggest

408 connectivity between the main stream and shallow groundwater, in agreement with observations in other glacierized

409 catchments (Hindshaw et al., 2011; Magnusson et al., 2014). However, a large spatio-temporal variability in the tracer

410 signal of springs was observed (Figs. 24) highlighting the complex hydrochemistry of the groundwater system (Brown

411 et al., 2006; Hindshaw et al., 2011; Kong and Pang, 2012). The depleted signal in summer months (Table 6) suggests a

412 role of snowmelt in groundwater recharge (Baraer et al., 2015; Fan et al., 2015; Xing et al., 2015) that was quantified in

413 a previous study (Penna et al., 2014). At the same time, the relatively high EC during summer demonstrates solute

414 concentration and suggests longer residence times and/or flow pathways (and thus long contact with the soil particles)

415 of infiltrating meltwater before recharging the groundwater (Brown et al., 2006; Esposito et al., 2016). The similar

416 coefficients of variations of the two tracers in summer and fall indicate less inter-seasonal differences in water inputs to

417 the springs compared to the streams and suggest continuous groundwater recharge even at the end of the melting

418 seasons, pointing out again to relatively long travel times and recharge times.

419

420 We mainly attribute the large spatial and temporal variability of tracers in stream water and groundwater to the control

421 exerted by climate (seasonality), topography and geological settings. For instance, the depleted waters at all locations in

422 June and early July 2012 (Fig. 3a) indicate heavy snowmelt contributions, consistent with the results of the mixing

423 models (Fig. 5), clearly reflecting a climatic control (snow accumulation during the winter-early spring and subsequent

424 melting). The increasing trend in EC from S8 to S1 during summer periods (Fig. 3b), consistent with other works (Kong

425 and Pang, 2012; Fan et al., 2015), reflects the combined effect of lower elevations, smaller snow-covered area,

426 decreasing glacierized area, progressive decrease of meltwater fractions and proportional increase of groundwater

427 contributions (Fig. 5), and inflows by groundwater-dominated lateral tributaries.

428 The more depleted median isotopic composition and the higher EC of S3-LSG (Fig. 2) reflected the influence of the

429 tributary T4, a few tens meter upstream of S3-LSG that had a depleted signal and very high EC and that plotted

430 separately in the mixing diagram (Fig. 4). A combination of depleted isotopic composition (typical of snowmelt) and

431 high EC (typical of groundwater) was very rare in the catchment, and we do not have evidence to explain the origin of

432 tributary T4 and the reason of its tracer signature. Analogously, our data did not provide robust explanations about the

433 more enriched isotopic composition and the constantly much lower EC of SPR4 compared to other springs (Figs. 3 and

434 4). Ongoing and future analyses of major anions and cations will help to shed some light on the origin of T4 and SPR4.

435

436 **5.2 Seasonal control on the δ^2H-EC relation and on meltwater fractions**

437 As observed elsewhere (e.g., Hindshaw et al., 2011; Maurya et al., 2011; Blaen et al., 2014), streamflow in the main

438 stream increased during melting periods, EC decreased due to the dilution effect and the isotopic composition generally

439 shifted towards depleted values reflecting the meltwater signal. However, the two tracers were strongly correlated only

440 in May, June and September (Fig. 7), when glacier melt was negligible or absent (Fig. 5) because the tracer signal in the

441 stream reflected the low EC and the depleted isotopic composition of snowmelt. Conversely, during mid-summer, when

442 glacier melt significantly contributed to streamflow (Fig. 5), the relation between the two tracers became weak (Fig. 7),

443 because glacier melt had very low EC but was not as isotopically depleted as snowmelt. Having multiple tracers is of

444 certain usefulness when investigating water sources and mixing processes (Barthold et al., 2011), especially in highly

445 heterogeneous environments (Hindshaw et al., 2011), and is essential for the identification of various streamflow

446 components. However, it is important to know the periods when only one tracer could be reliably used, at least for

447 assessing meltwater inputs, especially in glacierized catchments where logistical constraints are always challenging.

448

449 The hysteretic behaviour observed between streamflow and meltwater fraction for the melt-induced runoff events (Fig.

450 8) reflects the hysteresis observed in the relation between streamflow and EC (Engel et al., 2016), suggesting

451 contributions from water sources characterized by different temporal dynamics (Dzikowski and Jobard, 2012). The

452 combination of highest streamflow and highest meltwater proportion was obtained at both stream sections in June due

453 to the remarkable contribution of meltwater from the relatively deep snowpack in the upper part of the catchment. It is

454 worth to highlight how the meltwater fraction can frequently represent a substantial (> 50 %) proportion of the bankfull

455 discharge, both during snow and glacier melt flows. This implies that the expected progress of glacier shrinking and

456 future changes in both runoff components will likely have important consequences for the morphological configuration

457 of high-elevation streams like the Saldur River, especially in the wider, braided reaches more responsive to variations in

458 water and sediment fluxes (Wohl, 2010).

459

460 **5.3 Role of snowmelt and glacier melt on streamflow**

461 The spatial and temporal patterns of meltwater dynamics are consistent with those estimated in other high-elevation

462 catchments worldwide. For instance, the dominant role of snowmelt in late spring-early summer and of glacier melt

463 later in summer was observed across different sites in Asia, North America, South American and Europe (Aizen et al.,

464 1996; Cable et al., 2011; Ohlanders et al., 2013; Blaen et al., 2014, respectively). The decreasing contribution of

465 meltwater from the upper to the lower stream locations from June to October shown almost consistently by all scenarios

466 (Fig. 5) is related to the increasing distance from the glacier and catchment size, and decreasing elevation, in agreement

467 with results from other sites (Cable et al., 2011; Prasch et al., 2012; Racoviteanu et al., 2013; Marshall et al., 2014).

468 Moreover, lateral contributions from non-glacier fed tributaries and/or tributaries dominated by groundwater increased

469 the groundwater fraction in streamflow as well and proportionally decreased the meltwater fraction (Marshall et al.,

470 2014; Fan et al., 2015).

471

472 Our estimates of snowmelt contribution to streamflow during the melting season are consistent with those reported in

473 other studies (Carey and Quinton, 2004; Mukhopadhyay and Khan, 2015) and with those found in the same catchment

474 during individual runoff events (Engel et al., 2016). It is more difficult to compare our computed fractions of glacier

475 melt in stream water with estimates in other sites because they can be highly dependent on the yearly climatic

476 variability, on the proportion of glacierized area in the catchment and because they are usually reported at the monthly

477 or yearly scale. However, when considering the total meltwater contribution, the computed fractions for the June-

478 August period agree reasonably well with those recently estimated on a seasonal scale in other high-elevation

479 catchments by Pu et al. (2013) (41 - 62 %, 12 % of glacierized area), Fan et al. (2015) (26 - 69 %), Xing et al. (2015)

480 (almost 60 %) and at the annual scale by Jeelani et al. (2016) (52 %, 3 % of glacierized area), and are even higher than

481 those computed by Mukhopadhyay and Khan (2015) (25 - 36 %). These observations stress the importance of water

482 resources stored within the cryosphere even in catchments with limited extent of glacierized area, such as the Saldur

483 catchment.

484

Overall, our tracer-based results on the influence of snowmelt and glacier melt on streamflow agree with glacier mass balance results which revealed important losses from the glacier surface (-428 mm in snow water equivalent) for the year 2012-2013 (Galos, 2013). Particularly, the first strong heat wave serving as melting input was observed in mid-June, when the glacier was still covered by snow and no glacier melt occurred (Galos, 2013), in agreement with our estimates of snowmelt contributions (Fig. 5). Glaciological results also showed that most of the glacier mass loss occurred at the end of July to mid-August 2013, but glacier ablation in the lower part of the glacier (below 3000 m a.s.l.) was observed until the beginning of October (Galos, 2013), corroborating our tracer-based estimates (Fig. 5).

5.4 Sources of uncertainties in the estimated streamflow components

Various sources of uncertainty affect the estimate of the streamflow components when using mixing models in complex environments such as mountain catchments (Uhlenbrook and Hoeg, 2003; Ohlanders et al., 2013). In cases of mixing model applications to separate snowmelt from glacier melt and groundwater, thus not considering rainfall, and in the case of no availability of streamflow measurements (in our case at S8 and S1), uncertainty can be mainly ascribed to the precision of the instrument used for the determination of the tracer signal, and the spatio-temporal patterns of the end-member tracer signature. The instrumental precision can be relatively easily taken into account and quantified by adopting statistically-based procedures (e.g., Genereux et al., 1998). However, the spatio-temporal variation in the hydrochemical signal of the end-members is more challenging to capture and can provide the largest source of uncertainty (Uhlenbrook and Hoeg, 2003; Pu et al., 2013). The isotopic composition and EC of shallow groundwater emerging from springs can be very different within a catchment, especially in cases of heterogeneous geology, as well as the tracer signature of streams at different locations even during baseflow conditions (Jeelani et al., 2010; 2015). Indeed, in our case, the highest uncertainty in the estimated component fractions provided by scenarios A and C can likely be ascribed to the spatial variability of the tracer signature of the sampled springs.

The isotopic composition of snowmelt can mainly change according to i) macro-topography (e.g., aspect determines different melting rates and so different isotopic compositions); ii) micro-topography, because small hollows tend to host "older" snow with a more enriched isotopic composition compared to sloping areas; iii) elevation; and iv) season, with δ values becoming more negative with increasing elevation and more positive over the melting season (Uhlenbrook and Hoeg, 2003; Holko et al., 2013; Ohlanders et al., 2013). EC of snow, and therefore, snowmelt can change as well due, for instance, to the ionic pulse at the beginning of the melting season (Williams and Melack, 1991) and/or reflecting seasonal inputs of impurities from the atmosphere (Li et al., 2006), although this variability is usually much more limited compared to that of the isotopes.

In our case, the instrumental precision of the isotope analyser and the EC meter is relatively low and was entirely taken into account by the statistical assessment of uncertainty we applied. The spatio-temporal variability of snowmelt was addressed by sampling snowmelt at different elevations, aspects and times of the seasons. Finally, we observed very limited spatial-patterns but a marked seasonal change in the tracer signature of glacier melt (Table 5) that was taken into account in the mixing model application (Table 2). Despite these efforts, logistical issues related to the size of the catchment as well as practical and safety issues related to the accessibility of most areas of the catchment, not only in winter, and, not last, economical issues, prevent a very detailed characterization and quantification of all sources of uncertainty associated to the estimates of the streamflow components at different times of the year and different stream locations. In addition, an underestimation of meltwater fractions due to sampling time not always corresponding to the streamflow peak should be considered (Fig. 6). Specifically, the samples taken on June 19 at S5-USG and S3-LSG were

collected almost four hours before the streamflow peak. This means that an additional contribution of snowmelt almost up to 20 % could be expected (Fig. 6). As far as we know, these results have not been reported elsewhere and are critical for a proper assessment of the uncertainty in the estimated component fractions. Moreover, these observations suggest that adequate sampling strategies are critical (Uhlenbrook and Hoeg, 2003) and must be considered when planning field campaigns aiming at the quantification of meltwater in glacierized catchments.

5.6 Conceptual model of streamflow components dynamics

The findings from our two previous studies (Penna et al., 2014; Engel et al., 2016) and from the present work allow us to derive a conceptual model of streamflow and tracer response to meltwater dynamics in the Saldur catchment (Fig. 9). To the best of our knowledge, this is the first study to present such a conceptual model of streamflow component dynamics. Although intuitive, this conceptualization is important because it represents a paradigm that, given the characteristics of the study site, can be applied to many other glacierized catchments worldwide.

During late fall, winter and early spring, precipitation mainly falls in form of snow, streamflow reaches its minimum and is predominantly formed by baseflow. EC in stream water is highest and the isotopic composition is relatively enriched, reflecting the groundwater signal. In mid-spring the melting season begins. The snowpack starts to melt at the lower elevations in the catchment and the snow line progressively moves upwards; stream water EC begins to decrease due to the dilution effect and δ values become more negative, reflecting the first contribution of snowmelt (19 - 39 %). In late spring and early summer the combination of relatively high radiation inputs and still deep snowpack in the middle and upper portion of the catchment provides maximum snowmelt contributions to streamflow (up to 79 ± 6 % in the Saldur River at the highest sampling location) which is characterized by marked diurnal fluctuations and highest melt-induced peaks. Groundwater fractions in stream water become proportionally smaller. The glacier surface is still totally snow-covered, thus glacier melt does not appreciably contribute to streamflow. EC is very low due to the strong dilution effect and the isotopic composition is most depleted. In mid-summer the snowpack is present only at the highest elevations and the glacier surface is mostly snow-free, so that a combined role of snowmelt and glacier melt occurs. Streamflow is characterized by important diurnal fluctuations, but melt-induced peaks tend to be smaller in absolute values than in early summer associated with snowmelt. Although the snowmelt contribution has decreased, EC in the main stream is still very low due to the input of the extremely low EC of glacier melt. On the contrary, the stream water isotopic composition is less depleted compared to late spring and early summer due to the relatively more enriched signal of glacier melt with respect to snowmelt. In late summer snow disappears from most of the catchment and is only limited to residual patches in sheltered locations. The most important inputs to streamflow are provided by glacier melt that reaches its largest contributions (up to 68 - 71 % in the upper monitored Saldur River location). Diurnal fluctuations are still clearly visible but the decreasing radiation energy combined with lower melting supply limits high flows. EC begins to decrease and the isotopic composition to increase. From late spring to late summer low-intensity rainfall events provide limited contributions to streamflow. However, rainfall events of moderate or relatively higher intensity can occur so that rain-induced runoff superimposes the melt-induced runoff and produces the highest observed streamflow peaks. In early fall, meltwater contributions are limited to snowmelt from early snowfalls at high elevations and residual glacier melt and the groundwater proportions become progressively more important. Streamflow decreases significantly and only small diurnal fluctuations are observable during clear days. The two tracers slowly return to their background values.

6. Conclusions and future perspectives

566 Our tracer-based studies (water isotopes and EC) in the Saldur catchment aimed to investigate the water sources

567 variability and the contribution of snowmelt, glacier melt and groundwater to streamflow in order to contribute to a

568 better comprehension of the hydrology of high-elevation glacierized catchments. We highlighted the highly complex

569 hydrochemical signature of water in the catchment and the main controls on such variability. We applied mixing models

570 to estimate the fractions of meltwater in streamflow over a season, not only at the catchment outlet as usually performed

571 in other studies, but at different locations along the main stream. We found that snowmelt dominated the hydrograph in

572 late spring-early summer, with fractions ranging between 50 ± 5 % and 79 ± 6 % at different stream locations and

573 according to different model scenarios that took into account the spatial and temporal variability of end-member tracer

574 signature. Glacier melt was a remarkable streamflow component in August, with maximum contributions ranging

575 between 8 - 15 % and 68 - 71 % at different stream locations and according to different scenarios. These estimates

576 underline the key role of snowpack and glaciers on streamflow and stress their strategical importance as water

577 resources.

578

579 From a methodological perspective, our results showed that during mixed snowmelt and glacier melt periods, EC and

580 isotopes were not correlated due to the different tracer signature of the two sources of meltwater, whereas they provided

581 a consistent pattern during snowmelt periods only. Such a behaviour, that we found hardly reported elsewhere, should

582 be better assessed over longer time spans and in other sites, but suggests possible simplified monitoring strategies in

583 snow-dominated catchments or during snowmelt periods in glacierized catchments. We identified the main sources of

584 uncertainty in the computed estimates of streamflow components, mainly related to the spatio-temporal variability of

585 the end-member tracer signature, including a clear seasonal enrichment of glacier melt isotopic composition. This is a

586 pattern that must be considered when applying mixing models on a seasonal basis and that we invite to investigate in

587 other glacierized environments. Furthermore, this is the first study, to our knowledge, which quantified the possible

588 underestimation of meltwater fractions in streamflow occurring when stream water is sampled far from the streamflow

589 peak during melt-induced runoff events. Again, this raises awareness about the need of careful planning of tracer-based

590 field campaigns in high-elevation catchments.

591

592 We developed a perceptual model of meltwater dynamics and associated streamflow and tracer response in the Saldur

593 catchment that likely applies to many other glacierized catchments worldwide. However, some limitations intrinsic in

594 our approach should be considered. For instance, the reduced number of rain water samples collected at the rainfall-

595 event scale over the three years did not allow us to fully assess the seasonal role of precipitation on streamflow in

596 relation to meltwater. Furthermore, the use of EC, which integrates all water solutes in a single measurement, cannot

597 differentiate well some water sources and their relation with the underlying geology. Finally, the monthly sampling

598 resolution at different location is useful to obtain a general overview and first estimates of the seasonal variability of

599 streamflow components but high-frequency sampling can certainly help to capture finer hydrological dynamics. In this

600 context, the results of the present work can serve as a very useful basis for modelling applications, particularly to

601 constrain the model parametrization and to reduce the simulation uncertainties, and so to obtain more reliable

602 predictions of streamflow dynamics and meltwater contributions to streamflow in high-elevation catchments.

603

604 **Acknowledgements**

605 This work was supported by the research projects "Effects of climate change on high-altitude ecosystems: monitoring

606 the Upper Match Valley" (Foundation of the Free University of Bozen-Bolzano), "EMERGE: Retreating glaciers and

emerging ecosystems in the Southern Alps" (Dr. Erich Ritter- und Dr. Herzog-Sellenberg-Stiftung im Stifterverband für die Deutsche Wissenschaft), and partly by the project "HydroAlp", financed by the Autonomous Province of Bozen-Bolzano. We thank the Dept. of Hydraulic Engineering and Hydrographic Office of the Autonomous Province of Bozen-Bolzano for their technical support, G. Niedrist (EURAC) for maintaining the meteorological stations, Giulia Zuecco (University of Padova, Italy) for the isotopic analyses and Stefan Galos (University of Innsbruck, Austria) for sharing glacier mass balance results.

References

Aizen, V. B, Aizen, E. M., Melack, J. M, 1996. Precipitation, melt and runoff in the northern Tien Shan. Journal of Hydrology 186: 229–251.

Baraer, M., McKenzie, J., Mark, B.G., Gordon, R., Bury, J., Condom, T., Gomez, J., Knox, S., Fortner, S.K., 2015. Contribution of groundwater to the outflow from ungauged glacierized catchments: a multi-site study in the tropical Cordillera Blanca, Peru. Hydrological Processes 29, 2561–2581. doi:10.1002/hyp.10386

Barthold, F.K., Tyralla, C., Schneider, K., Vaché, K.B., Frede, H.-G., Breuer, L., 2011. How many tracers do we need for end member mixing analysis (EMMA)? A sensitivity analysis. Water Resources Research 47, W08519. doi:10.1029/2011WR010604

Beniston, M., 2012. Impacts of climatic change on water and associated economic activities in the Swiss Alps. Journal of Hydrology 412-413, 291–296. doi:10.1016/j.jhydrol.2010.06.046

Blaen, P.J., Hannah, D.M., Brown, L.E., Milner, A.M., 2014. Water source dynamics of high Arctic river basins: water source dynamics of high arctic river basins. Hydrological Processes 28, 3521–3538. doi:10.1002/hyp.9891

Brown, L.E., Hannah, D.M., Milner, A.M., Soulsby, C., Hodson, A.J., Brewer, M.J., 2006. Water source dynamics in a glacierized alpine river basin (Taillon-Gabiétous, French Pyrénées): alpine basin water source dynamics. Water Resources Research 42, W08404, doi:10.1029/2005WR004268

Cable, J., Ogle, K., Williams, D., 2011. Contribution of glacier meltwater to streamflow in the Wind River Range, Wyoming, inferred via a Bayesian mixing model applied to isotopic measurements. Hydrological Processes 25, 2228–2236. doi:10.1002/hyp.7982

Carey, S.K., Quinton, W.L., 2004. Evaluating snowmelt runoff generation in a discontinuous permafrost catchment using stable isotope, hydrochemical and hydrometric data. Nordic hydrology 35, 309–324.

Carey, S.K., Quinton, W.L., 2005. Evaluating runoff generation during summer using hydrometric, stable isotope and hydrochemical methods in a discontinuous permafrost alpine catchment. Hydrological Processes 19, 95–114. doi:10.1002/hyp.5764

Carturan, L., Zuecco, G., Seppi, R., Zanoner, T., Borga, M., Carton, A., Dalla Fontana, G. Catchment-scale permafrost mapping using spring water characteristics. Permafrost and Periglacial Processes, in press. doi: 10.1002/ppp.1875.

Dzikowski, M., Jobard, S., 2012. Mixing law versus discharge and electrical conductivity relationships: application to an alpine proglacial stream. Hydrological Processes 26, 2724–2732. doi:10.1002/hyp.8366

Engel, M., Penna, D., Bertoldi, G., Dell'Agnese, A., Soulsby, C., Comiti, F., 2016. Identifying run-off contributions during melt-induced run-off events in a glacierized alpine catchment: Hydrological Processes, 30: 343–364. doi:10.1002/hyp.10577

Engelhardt, M., Schuler, T.V., Andreassen, L.M., 2014. Contribution of snow and glacier melt to discharge for highly glacierised catchments in Norway. Hydrology and Earth System Sciences 18, 511–523. doi:10.5194/hess-18-511-2014

648   Esposito, A., Engel, M., Ciccazzo, S., Daprà, L., Penna, D., Comiti, F., Zerbe, S., Brusetti, L., 2016. Spatial and
649   temporal variability of bacterial communities in high alpine water spring sediments. Research in Microbiology
650   167, 325–333. doi:10.1016/j.resmic.2015.12.006

651   Fan, Y., Chen, Y., Li, X., Li, W., Li, Q., 2015. Characteristics of water isotopes and ice-snowmelt quantification in the
652   Tizinafu River, north Kunlun Mountains, Central Asia. Quaternary International 380-381, 116–122.
653   doi:10.1016/j.quaint.2014.05.020

654   Finger, D., Hugentobler, A., Huss, M., Voinesco, A., Wernli, H., Fischer, D., Weber, E., Jeannin, P.-Y., Kauzlaric, M.,
655   Wirz, A., Vennemann, T., Hüsler, F., Schädler, B., Weingartner, R., 2013. Identification of glacial meltwater
656   runoff in a karstic environment and its implication for present and future water availability. Hydrology and Earth
657   System Sciences 17, 3261–3277. doi:10.5194/hess-17-3261-2013

658   Fischer, B.M.C., Rinderer, M., Schneider, P., Ewen, T., Seibert, J., 2015. Contributing sources to baseflow in pre-alpine
659   headwaters using spatial snapshot sampling. Hydrological Processes. doi:10.1002/hyp.10529

660   Galos S., 2013. The mass balance of Matscherferner 2012/13. Report of the research project "A physically based regional
661   mass balance approach for the glaciers of Vinschgau – glacier contribution to water availability", funded by the
662   Autonomous Province of Bozen-Bolzano, Italy.

663   Genereux D., 1998. Quantifying uncertainty in tracer-based hydrograph separations. Water Resources Research, 34(4),
664   915–919 .doi:10.1029/98WR00010.

665   Hindshaw, R.S., Tipper, E.T., Reynolds, B.C., Lemarchand, E., Wiederhold, J.G., Magnusson, J., Bernasconi, S.M.,
666   Kretzschmar, R., Bourdon, B., 2011. Hydrological control of stream water chemistry in a glacial catchment
667   (Damma Glacier, Switzerland). Chemical Geology 285, 215–230. doi:10.1016/j.chemgeo.2011.04.012

668   Hoeg, S., Uhlenbrook, S. and Leibundgut, C., 2000. Hydrograph separation in a mountainous catchment - combining
669   hydrochemical and isotopic tracers. Hydrological Processes, 14: 1199–1216. doi: 10.1002/(SICI)1099-
670   1085(200005)14:7<1199::AID-HYP35>3.0.CO;2-K.

671   Holko, L., Danko, M., Dóša, M., Kostka, Z., Šanda, M., Pfister, L., Iffly, J.F., 2013. Spatial and temporal variability of
672   stable water isotopes in snow related hydrological processes. Die Bodenkultur 39, 3–4.

673   Jeelani, G., Bhat, N.A., Shivanna, K., 2010. Use of δ^{18}O tracer to identify stream and spring origins of a mountainous
674   catchment: A case study from Liddar watershed, Western Himalaya, India. Journal of Hydrology 393, 257–264.
675   doi:10.1016/j.jhydrol.2010.08.021

676   Jeelani, G., Kumar, U.S., Bhat, N.A., Sharma, S., Kumar, B., 2015. Variation of δ^{18}O, δD and 3H in karst springs of
677   south Kashmir, western Himalayas (India). Hydrological Processes 29, 522–530. doi:10.1002/hyp.10162

678   Jeelani, G., Shah, R. A., Jacob, N., Deshpande, R. D., 2016. Estimation of snow and glacier melt contribution to Liddar
679   stream in a mountainous catchment, western Himalaya: an isotopic approach. Isotopes in Environmental and
680   Health Studies. doi: 10.1080/10256016.2016.1186671

681   Jost, G., Moore, R.D., Menounos, B., Wheate, R., 2012. Quantifying the contribution of glacier runoff to streamflow in
682   the upper Columbia River Basin, Canada. Hydrology and Earth System Sciences 16, 849–860. doi:10.5194/hess-
683   16-849-2012

684   Jouzel, J., Souchez, R. A., 1982. Melting-refreezing at the glacier sole and the isotopic composition of the ice. Journal
685   of Glaciology 28(98): 35–42.

686   Kendall, C., McDonnell, J. J., 1998. Isotope tracers in catchment hydrology. Elsevier Science Limiter, Amsterdam.

687   Klaus, J., McDonnell, J.J., 2013. Hydrograph separation using stable isotopes: Review and evaluation. Journal of
688   Hydrology 505, 47–64. doi:10.1016/j.jhydrol.2013.09.006

689 Kong, Y., Pang, Z., 2012. Evaluating the sensitivity of glacier rivers to climate change based on hydrograph separation
690   of discharge. Journal of Hydrology 434-435, 121–129. doi:10.1016/j.jhydrol.2012.02.029

691 Lee, J., Feng, X., Faiia, A.M., Posmentier, E.S., Kirchner, J.W., Osterhuber, R., Taylor, S., 2010. Isotopic evolution of a
692   seasonal snowcover and its melt by isotopic exchange between liquid water and ice. Chemical Geology 270, 126–
693   134. doi:10.1016/j.chemgeo.2009.11.011

694 Li, Zhongqin, Ross, Edwards, Mosley-Thompson, E., Wang, Feiteng, Dong, Zhibao, You, Xiaoni, Li, Huilin, Li, Zhu,
695   Chuanjin, Yuman, 2006. Seasonal variabilities of ionic concentration in surface snow and elution process in snow-
696   firn packs at PGPI Site on Glacier No.1 in Eastern Tianshan, China. Annals of Glaciology, 43A075.

697 Magnusson, J., Kobierska, F., Huxol, S., Hayashi, M., Jonas, T., Kirchner, J.W., 2014. Melt water driven stream and
698   groundwater stage fluctuations on a glacier forefield (Dammagletscher, Switzerland): stream-groundwater
699   interactions on a glacier forefield. Hydrological Processes 28, 823–836. doi:10.1002/hyp.9633

700 Mair E., Leitinger G., Della Chiesa S., Niedrist G., Tappeiner U., Bertoldi G., 2015. A simple method to combine snow
701   height and meteorological observations to estimate winter precipitation at sub-daily resolution. Hydrological
702   Sciences Journal. doi:10.1080/02626667.2015.1081203

703 Mao, L., Dell'Agnese, A., Huincache, C., Penna, D., Engel, M., Niedrist, G., Comiti, F., 2014. Bedload hysteresis in a
704   glacier-fed mountain river: bedload hysteresis in a glacier-fed mountain river. Earth Surface Processes and
705   Landforms 39, 964–976. doi:10.1002/esp.3563

706 Marshall, S.J., 2014. Meltwater run-off from Haig Glacier, Canadian Rocky Mountains, 2002-2013. Hydrology and
707   Earth System Sciences 18, 5181–5200. doi:10.5194/hess-18-5181-2014

708 Maurya, A.S., Shah, M., Deshpande, R.D., Bhardwaj, R.M., Prasad, A., Gupta, S.K., 2011. Hydrograph separation and
709   precipitation source identification using stable water isotopes and conductivity: River Ganga at Himalayan
710   foothills. Hydrological Processes 25, 1521–1530. doi:10.1002/hyp.7912

711 Mukhopadhyay, B., Khan, A., 2015. A reevaluation of the snowmelt and glacial melt in river flows within Upper Indus
712   Basin and its significance in a changing climate. Journal of Hydrology 527, 119–132.
713   doi:10.1016/j.jhydrol.2015.04.045

714 Mutzner, R., Weijs, S.V., Tarolli, P., Calaf, M., Oldroyd, H.J., Parlange, M.B., 2015. Controls on the diurnal
715   streamflow cycles in two subbasins of an alpine headwater catchment. Water Resources Research 51, 3403–3418.
716   doi:10.1002/2014WR016581

717 Ogunkoya O. O., Jenkins A., 1993. Analysis of storm hydrograph and flow pathways using a three-component
718   hydrograph separation model. Journal of Hydrology 142: 71–88.

719 Ohlanders, N., Rodriguez, M., McPhee, J., 2013. Stable water isotope variation in a Central Andean watershed
720   dominated by glacier and snowmelt. Hydrology and Earth System Sciences 17, 1035–1050. doi:10.5194/hess-17-
721   1035-2013

722 Penna, D., Engel, M., Mao, L., Dell'Agnese, A., Bertoldi, G., Comiti, F., 2014. Tracer-based analysis of spatial and
723   temporal variations of water sources in a glacierized catchment. Hydrology and Earth System Sciences 18, 5271–
724   5288. doi:10.5194/hess-18-5271-2014

725 Penna, D., Stenni, B., Šanda, M., Wrede, S., Bogaard, T.A., Gobbi, A., Borga, M., Fischer, B.M.C., Bonazza, M.,
726   Chárová, Z., 2010. On the reproducibility and repeatability of laser absorption spectroscopy measurements for δ^2H
727   and $\delta^{18}O$ isotopic analysis. Hydrology and Earth System Sciences 14, 1551–1566. doi:10.5194/hess-14-1551-2010

728 Penna, D., Stenni, B., Šanda, M., Wrede, S., Bogaard, T.A., Michelini, M., Fischer, B.M.C., Gobbi, A., Mantese, N.,
729   Zuecco, G., Borga, M., Bonazza, M., Sobotková, M., Čejková, B., Wassenaar, L.I., 2012. Technical Note:

730   Evaluation of between-sample memory effects in the analysis of δ^2H and δ^{18}O of water samples measured by laser
731   spectroscopes. Hydrology and Earth System Sciences 16, 3925–3933. doi:10.5194/hess-16-3925-2012

732 Penna, D., van Meerveld, H.J., Oliviero, O., Zuecco, G., Assendelft, R.S., Dalla Fontana, G., Borga, M., 2015. Seasonal
733   changes in runoff generation in a small forested mountain catchment. Hydrological Processes 29, 2027–2042.
734   doi:10.1002/hyp.10347

735 Pinder G. F., Jones J. F., 1969. Determination of ground-water component of peak discharge from chemistry of total
736   runoff. Water Resources Research, 5(2), 438–445, doi: 10.1029/WR005i002p00438.

737 Prasch, M., Mauser, W., Weber, M., 2013. Quantifying present and future glacier melt-water contribution to runoff in a
738   central Himalayan river basin. The Cryosphere 7, 889–904. doi:10.5194/tc-7-889-2013

739 Pu, T., He, Y., Zhu, G., Zhang, N., Du, J., Wang, C., 2013. Characteristics of water stable isotopes and hydrograph
740   separation in Baishui catchment during the wet season in Mt. Yulong region, south western China. Hydrological
741   Processes 27, 3641–3648. doi:10.1002/hyp.9479

742 Racoviteanu, A.E., Armstrong, R., Williams, M.W., 2013. Evaluation of an ice ablation model to estimate the
743   contribution of melting glacier ice to annual discharge in the Nepal Himalaya. Water Resources Research 49,
744   5117–5133. doi:10.1002/wrcr.20370

745 Rock, L., Mayer, B., 2007. Isotope hydrology of the Oldman River basin, southern Alberta, Canada. Hydrological
746   Processes 21, 3301–3315. doi:10.1002/hyp.6545

747 Schaefli, B., Hingray, B., Musy, A., 2007. Climate change and hydropower production in the Swiss Alps: quantification
748   of potential impacts and related modelling uncertainties. Hydrology and Earth System Sciences Discussions 11,
749   1191–1205.

750 Sklash M. G., 1990. Environmental isotope studies of storm and snowmelt runoff generation. In Anderson, M. G., and
751   Burt, T. P., editors: Process studies in hillslope hydrology. Chichester: Wiley, 401-35.

752 Sklash M. G., Farvolden R. N., 1979. Role of groundwater in storm runoff. Journal of Hydrology, 43(1–4), 45–65, doi:
753   10.1016/0022-1694(79)90164-1.

754 Stichler, W., Schotterer, U., Fröhlich, K., Ginot, P., Kull, C., Gäggeler, H., Pouyaud, B., 2001. Influence of sublimation
755   on stable isotope records recovered from high-altitude glaciers in the tropical Andes. Journal of Geophysical
756   Research 106, 22613–22620.

757 Taylor, S., Feng, X., Kirchner, J.W., Osterhuber, R., Klaue, B., Renshaw, C.E., 2001. Isotopic evolution of a seasonal
758   snowpack and its melt. Water Resources Research 37, 759–769.

759 Uhlenbrook, S., Hoeg, S., 2003. Quantifying uncertainties in tracer-based hydrograph separations: a case study for two-,
760   three- and five-component hydrograph separations in a mountainous catchment. Hydrological Processes 17, 431–
761   453. doi:10.1002/hyp.1134

762 Vaughn, B. H., Fountain, A. G., 2005. Stable isotopes and electrical conductivity as keys to understanding water
763   pathways and storage in South Cascade Glacier, Washington, USA. Annals of Glaciology, 40, 1, 107-112, doi:
764   10.3189/172756405781813834

765 Williams, M. W., Melack, J. M., 1991. Solute chemistry of snowmelt and runoff in an Alpine Basin, Sierra Nevada,
766   Water Resour. Res., 27(7), 1575–1588, doi:10.1029/90WR02774.

767 Wohl E., 2010. Mountain rivers revisited, volume 19. ISBN: 978-0-87590-323-1, American Geophysical Union.

768 Xing, B., Liu, Z., Liu, G., Zhang, J., 2015. Determination of runoff components using path analysis and isotopic
769   measurements in a glacier-covered alpine catchment (upper Hailuogou Valley) in southwest China: hydrograph

770   separation; path analysis; glacier-covered catchment. Hydrological Processes 29, 3065–3073.

771   doi:10.1002/hyp.10418

772   Yde, J.C., Knudsen, N.T., Steffensen, J.P., Carrivick, J.L., Hasholt, B., Ingeman-Nielsen, T., Kronborg, C., Larsen,

773   N.K., Mernild, S.H., Oerter, H., Roberts, D.H., Russell, A.J., 2016. Stable oxygen isotope variability in two

774   contrasting glacier river catchments in Greenland. Hydrology and Earth System Sciences 20, 1197–1210.

775   doi:10.5194/hess-20-1197-2016

776   Yuanqing H, Theakstone WH, Tandong Y, Yafeng S., 2001. The isotopic record at an alpine glacier and its implications

777   for local climatic changes and isotopic homogenization processes. Journal of Glaciology, 47(156):147-151.

778   doi:10.3189/172756501781832601

779   Zhou, S., Wang, Z. and Joswiak, D. R., 2014. From precipitation to runoff: stable isotopic fractionation effect of glacier

780   melting on a catchment scale. Hydrological Process., 28: 3341–3349. doi: 10.1002/hyp.9911

Tables

Table 1. Sampling years and number of samples collected from the different water sources and used in this study.

Water source	ID of sampling locations	Sampling years	Total n. of samples
Snowmelt	-	2011-2013	24
Glacier melt	-	2012-2013	16
Stream (main river)	S1-S8	2011-2012	535
	S1, S3-LSG, S5-USG, S8	2013	
Stream (tributaries)	T1	2012	102
	T2, T4, T5	2011-2013	
	T3	2011	
Spring	SPR1-SPR4	2011-2013	84
	SPR6, SPR7	2013	

Table 2. Summary of the properties of the end-members used in the four mixing model scenarios for 2013 data.

Scenario	Groundwater end-member	Snowmelt end-member	Glacier melt end-member
A	Average δ^2H and EC of samples taken from selected springs in fall (2011-2013)	Time-invariant isotopic composition and EC (2013)	Monthly-variable isotopic composition and EC (2013)
B	Average δ^2H and EC of samples taken at each stream location in fall and winter (2011-2013)		
C	Average δ^2H and EC of samples taken from selected springs in fall (2011-2013)	Monthly-variable isotopic composition and EC (2013)	
D	Average δ^2H and EC of samples taken at each stream location in fall and winter (2011-2013)		

Table 3. Isotopic composition (δ^2H) and EC of the groundwater end-member used in the two- and three-component mixing model for the four scenarios for 2013 data. n: number of samples; avg.: average; SD: standard deviation.

	δ^2H (‰)						EC (µS/cm)					
	Scenarios A and C			Scenarios B and D			Scenarios A and C			Scenarios B and D		
Sampling location	n	avg.	SD	n	avg.	SD	n	avg.	SD	n	avg.	SD
S1	7	-101.7	5.7	5	-101.5	2.8	7	317.7	76.6	5	257.0	11.4
S3-LSG				3	-101.7	1.4				3	298.0	6.6
S5-USG	5	-98.5	1.3	4	-101.6	3.0	5	288.2	40.7	4	220.4	19.0
S8				1	-101.8	(-) 0.5*				1	210.0	(-) 0.1*

*For S8 only one sample was collected during baseflow conditions due to the difficult accessibility of the location in fall and winter. Therefore, no standard deviation could be computed, and the instrumental precision was used for the computation of the uncertainty of the estimated fractions.

Table 4. Isotopic composition (δ^2H) and EC of the snowmelt end-member used in the two- and three-component mixing model for the four scenarios for 2013 data. Abbreviations are used as in Table 2.

| | δ²H (‰)* | | | | EC (µS/cm) | | | | | |
| | Scenarios A and B | | Scenarios C and D | | Scenarios A and B | | | Scenarios C and D | | |
Sampling day	n	avg.	N	avg.	n	avg.	SD	n	avg.	SD
23 May			1	-195.4				1	15.3	(-) 0.1***
19 June			7	-160.1				7	11.9	22.1
16 July	7	-160.1	3	-134.3	13	10.9	17.1	3	12.5	14.7
12 Aug.										
11 Sept.**			2	-139.9				2	2.9	0.4
18 Oct.**										

*Because the isotopic composition of the high-elevation snowmelt end-member derived by a regression (Eq. 11), the standard deviation was not computed. Thus, the computation of uncertainty was based on the standard error of the estimate of the regression (6.0 ‰) instead of the standard deviation of the samples averaged for each month.

**Because no snowmelt samples were collected in September and October, the August value was used also for the two sampling days in September and October.

***In May 2013, only one snowmelt sample was collected. Therefore, no standard deviation could be computed, and the instrumental precision was used for the computation of the uncertainty of the estimated fractions.

Table 5. Isotopic composition (δ^2H) and EC of the glacier melt end-member used in the three-component mixing model for all scenarios for 2013 data. Abbreviations are used as in Table 2.

| | δ²H (‰) | | | EC (µS/cm) | | |
Sampling day	n	avg.	SD	n	avg.	SD
16 July	3	-110.7	1.5	3	2.0	0.3
12 Aug.	2	-104.2	3.8	2	2.2	0.7
11 Sept.	2	-92.6	6.5	2	2.5	1.8
18 Oct.*	2	-89.6	4.5	2	2.7	1.7

*No samples were collected on 18 October, when the stream was sampled. Therefore, the tracer value of the glacier melt samples collected on 26 September was used in the mixing model calculations.

Table 6. Basic statistics of isotopic composition (^{2}H) and EC of stream water in the Saldur catchment for data collected in the three sampling years. CV: coefficient of variation. The other abbreviations are used as in Table 2. Note that for simplicity the negative sign from the coefficient of variation of isotope data was removed.

Period*	Statistic	δ^2H Saldur River (‰)	δ^2H tributaries (‰)	δ^2H springs (‰)	EC Saldur River (µS/cm)	EC tributaries (µS/cm)	EC springs (µS/cm)
Entire period	N	274	102	80	257	102	74
	avg.	-105.3	-103.4	-105.5	166.5	226.8	227.7
	SD	5.2	4.9	6.1	57.1	104.0	77.8
	CV	0.049	0.047	0.058	0.343	0.459	0.342
Summer	N	240	81	68	223	81	62
	avg.	-105.9	-104.5	-107.0	153.7	218.5	229.7
	SD	5.3	4.5	5.1	48.3	100.6	78.3
	CV	0.050	0.043	0.048	0.314	0.460	0.341
Fall-winter	N	34	21	12	34	21	12
	avg.	-101.1	-99.2	-96.9	250.7	258.8	217.2
	SD	2.6	4.0	4.2	32.9	113.0	77.8
	CV	0.026	0.040	0.044	0.131	0.437	0.358

* Summer is considered between mid-June (21) and end of September (23), and fall-winter between end of September and end of March (21).

Table 7. Basic statistics of specific discharge, δ^2H and EC for the two groups reported in Fig. 7 for data collected in the three sampling years. Abbreviations are used as in Table 2.

	May, June, Sept. 2011-2013				July, August 2011-2013			
	q (m³/s/km²)	δ^2H (‰)	EC (µS/cm)	T (°C)	q (m³/s/km²)	δ^2H (‰)	EC (µS/cm)	T (°C)
n	12	12	12	12	12	12	12	12
avg.	0.08	-109.3	193.5	5.9	0.15	-107.0	118.3	11.6
SD	0.09	5.2	52.7	5.4	0.04	5.6	25.7	1.0

Figures
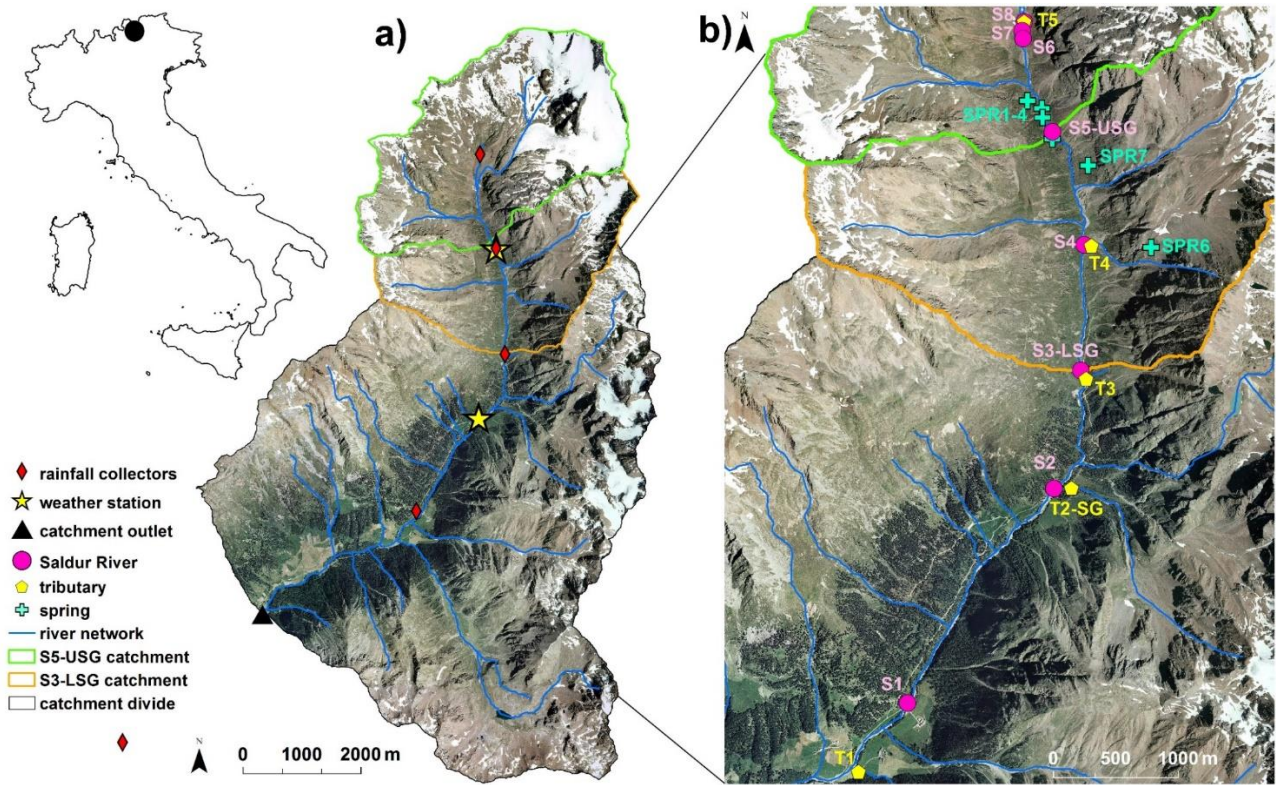
Figure 1. Map of the Saldur catchment, with its localization in the country, and position of field instruments and sampling points. Data from the rainfall collectors were not used in this study but their position is reported for completeness.
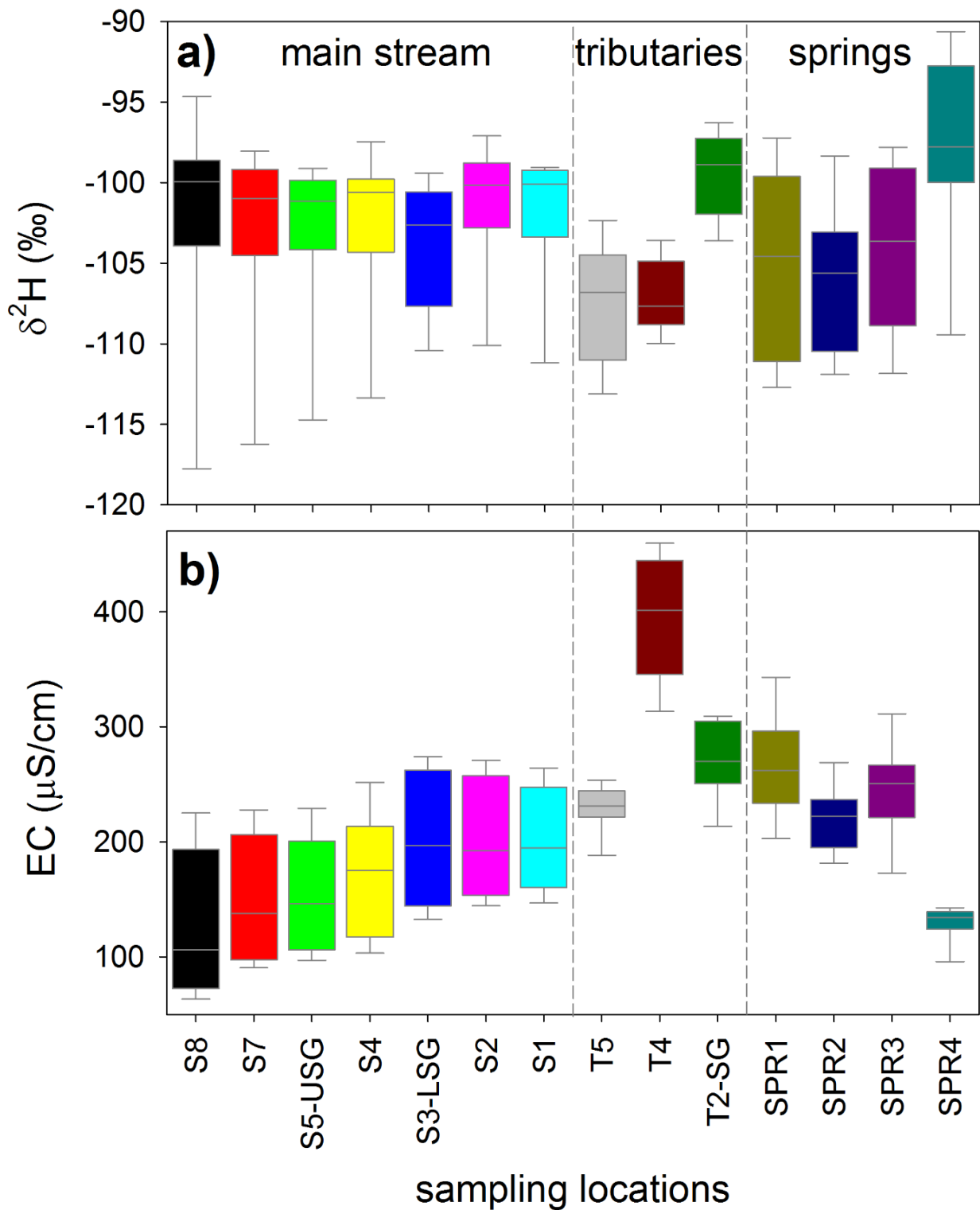
Figure 2. Box-plot of δ^2H (panel a)) and EC (panel b)) for samples taken on the same day at all locations in 2011 and 2012 (n = 10 for all locations except for isotope data in T5 and for both tracers at SPR1, for which n = 9). Locations T1 and T3 are excluded because sampled only for one year. The boxes indicate the 25th and 75th percentile, the whiskers indicate the 10th and 90th percentile, the horizontal line within the box defines the median. In 2013 samples were collected only at some locations (Table 1) and therefore, for consistency, 2013 data are not reported here.
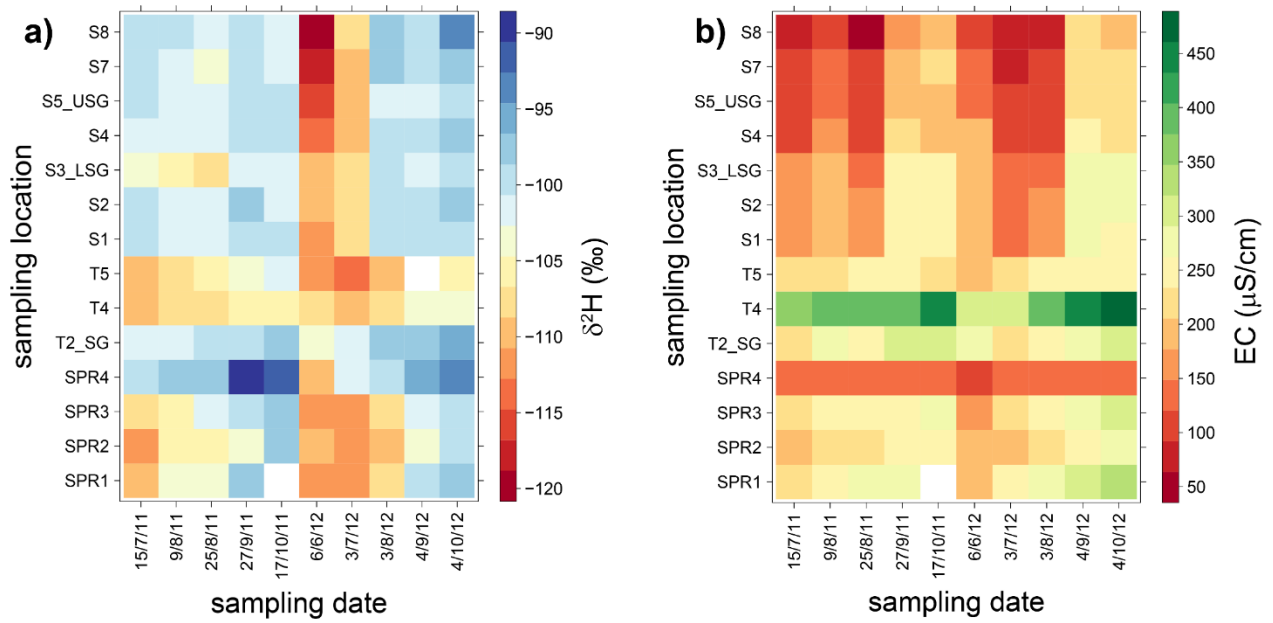
Figure 3. Spatio-temporal patterns of δ^2H (panel a)) and EC (panel b)) for samples taken on the same day at all locations in 2011 and 2012. Location T1 and T3 are excluded because sampled only for one year. White cells indicate no available measurements. In 2013 samples were collected only at some locations (Table 1) and therefore, for consistency, 2013 data are not reported here.
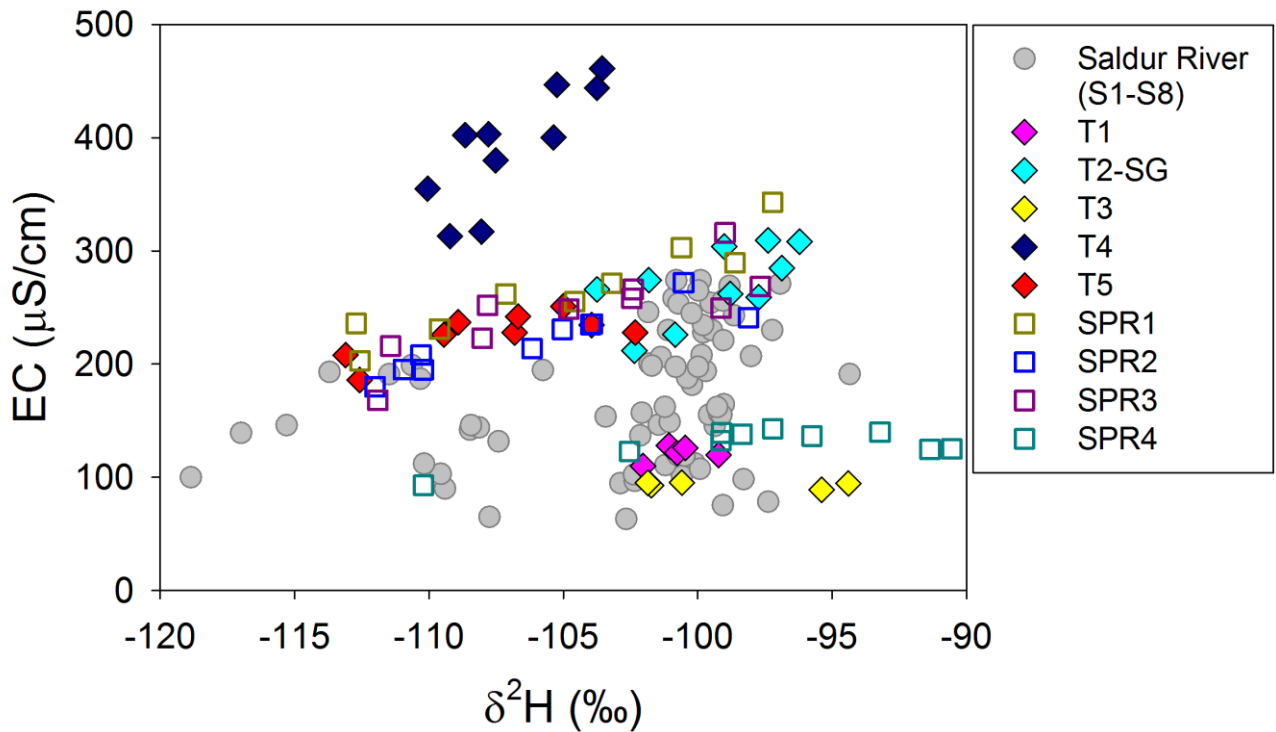
Figure 4. Relation between δ^2H and EC at all locations in the main stream, the tributaries and the springs in 2011 and 2012. Data refer to samples collected at each location on the same days except for T1 and T3, where samples were taken for one year only (cf. Table 1). In 2013 samples were collected only at some locations (Table 1) and therefore, for consistency, 2013 data are not reported here.
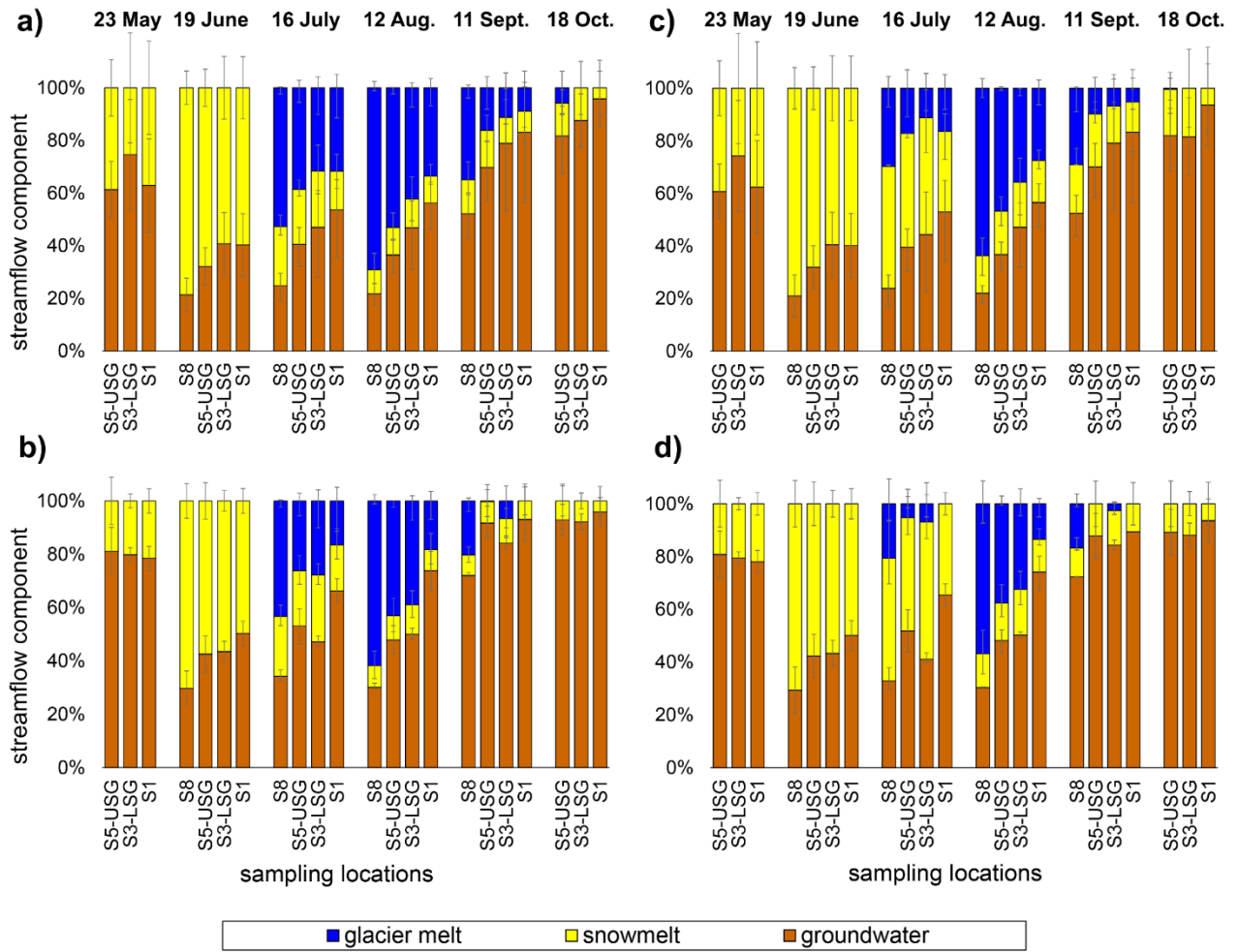
Figure 5. Fractions of groundwater, snowmelt and glacier melt in streamflow for the six sampling days in 2013 at four cross sections along the Saldur River. Left column: the isotopic composition and EC of the snowmelt end-member was considered time invariant, and the groundwater end-member was based on spring data (scenario A, panel a)) or on stream data (scenario B, panel b)). Right column: the isotopic composition of the snowmelt end-member was considered monthly-variable, and the groundwater end-member was based on spring data (scenario C, panel c)) or on stream data (scenario D, panel d)). The error bars represent the statistical uncertainty for each component.
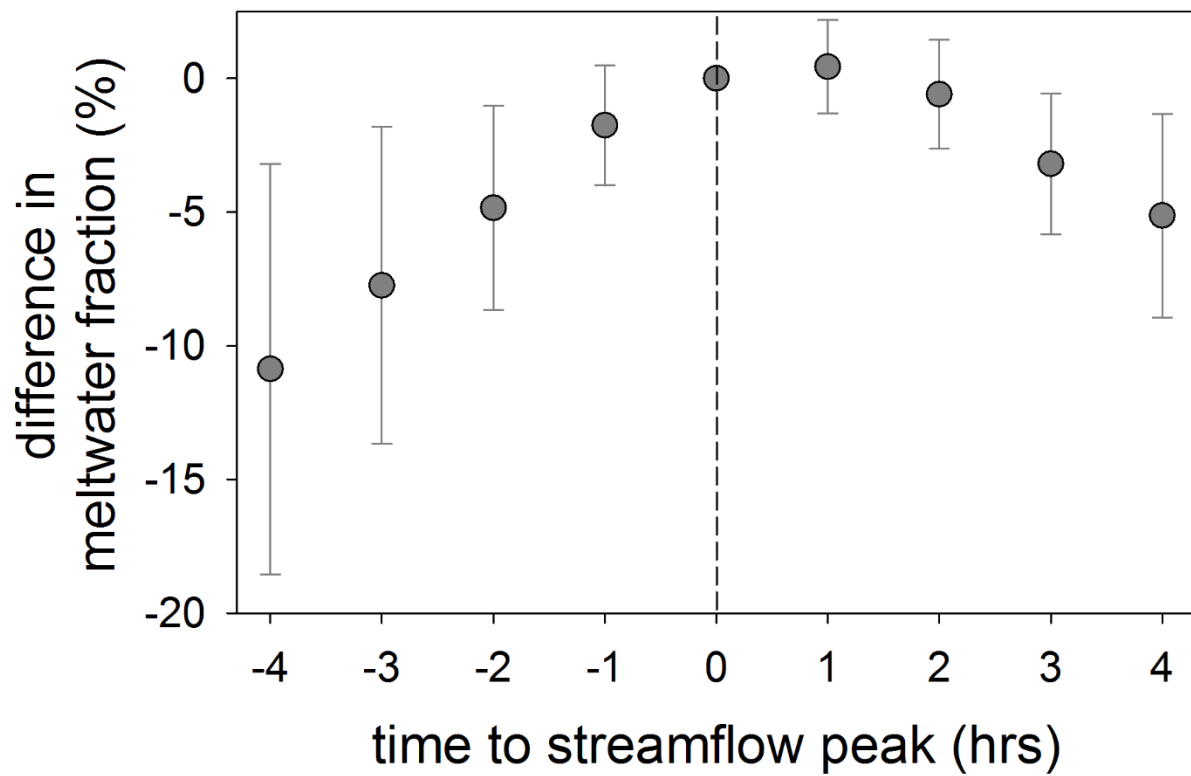
Figure. 6. Average difference between the meltwater fraction in streamflow at the time of streamflow peak and the meltwater fraction at different hours from the time of streamflow peak for the melt-induced runoff events at S5-USG and S3-LSG in 2011-2013. Error bars represent the standard deviation. The vertical line indicates the time of streamflow peak.
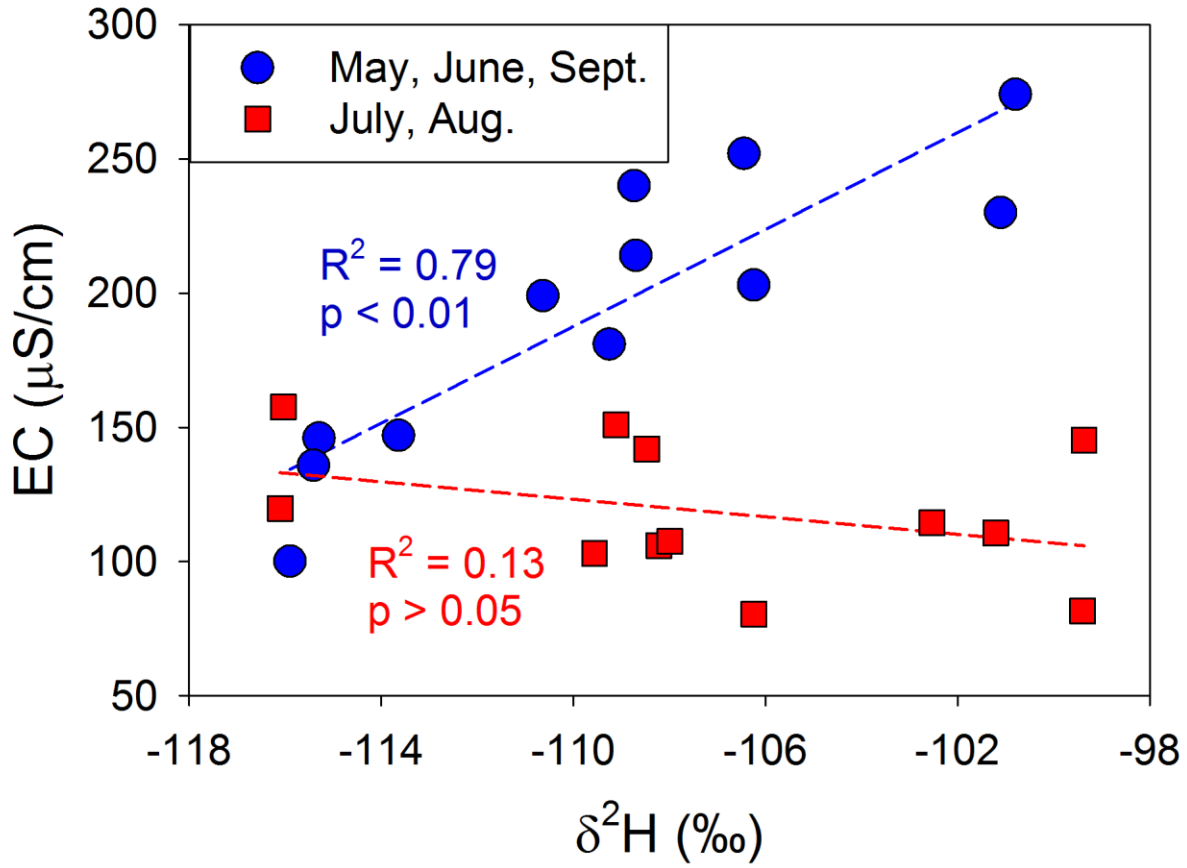
Figure 7. Relation between δ^2H and EC of samples collected at S5-USG and S3-LSG on the same days in 2011, 2012 and 2013, grouped by month.
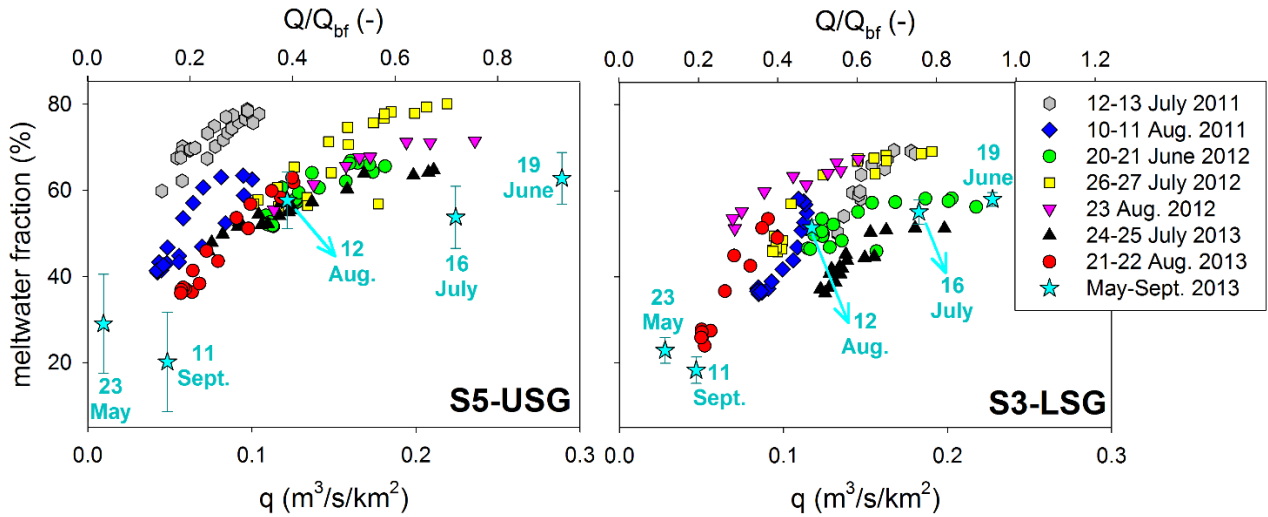
Figure 8. Relation between specific discharge (q) and meltwater fraction (%) in streamflow for the melt-induced runoff events in 2011, 2012 and 2013 sampled at hourly time scale (represented by different coloured symbols), and for the monthly sampling days in 2013 at S5-USG and S3-LSG (represented by stars in cyan). Meltwater fractions for the melt-induced runoff events were taken from Engel et al., (2016), while meltwater fractions for the monthly sampling days in 2013 are given by the average of the four different mixing models scenarios (presented in Fig. 5), and error bars indicate the standard deviation. For the double-peak event on 23-24 August 2012 at S5-USG, where a 9 mm rainstorm superimposed the melt event (c.f. Engel et al., 2016), only the melt-induced part of the event was considered. Discharge is reported also as fraction of the bankfull discharge Q_{bf} at the two sections.
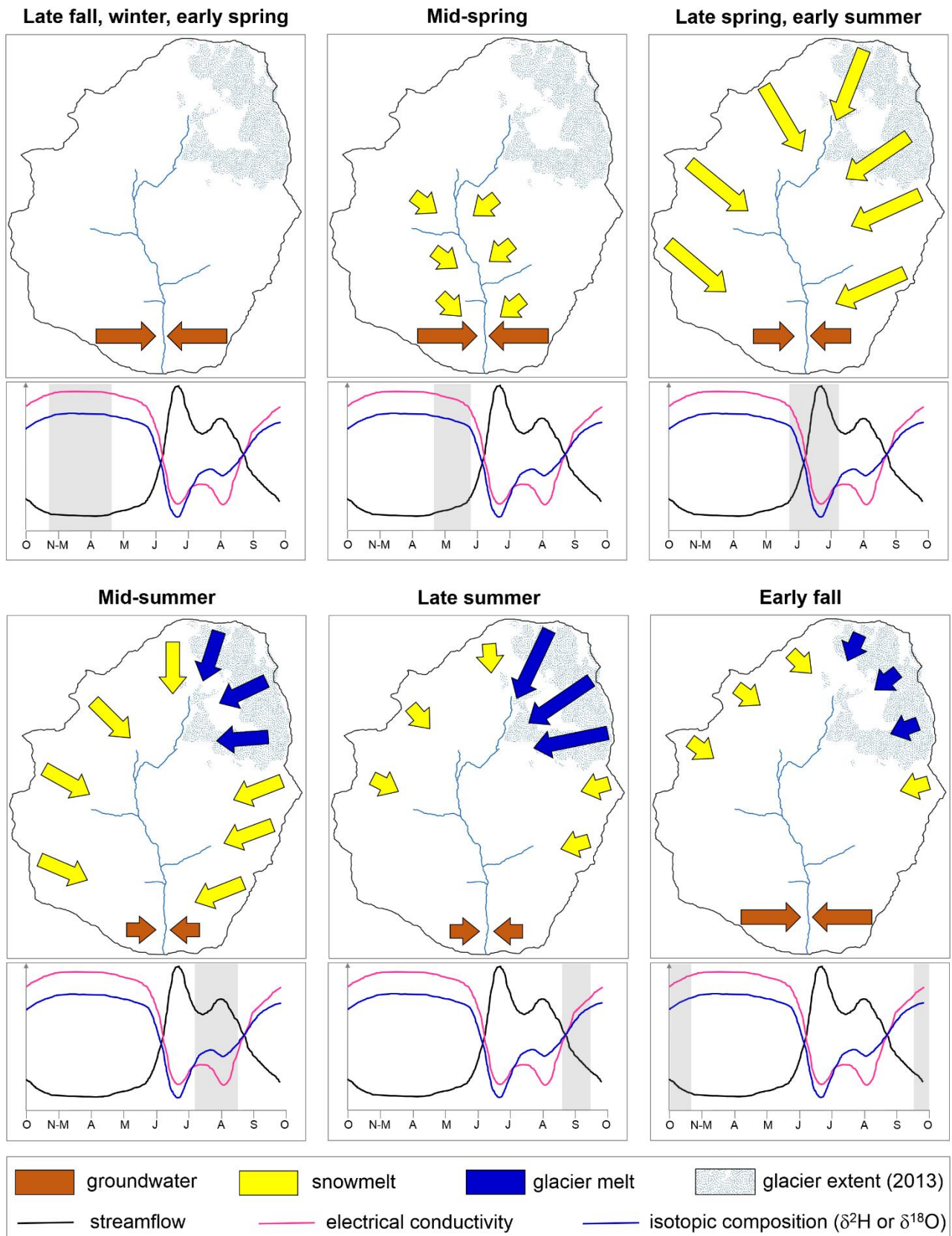
Figure 9. Conceptual model of contributions to streamflow in the Saldur River catchment (closed at LSG). The top subplots in each panel represent the water contributions to streamflow, and the bottom subplots show a sketch hydrograph along with EC and isotopic composition of stream water. The size of the arrows is roughly proportional to the intensity of water fluxes.